REPUBLIC OF TURKEY
ADANA ALPARSLAN TÜRKEŞ SCIENCE AND TECHNOLOGY UNIVERSITY

INSTITUTE OF GRADUATE SCHOOL
DEPARTMENT OF MECHANICAL ENGINEERING

DESIGN, MODELLING, AND DYNAMIC SIMULATION OF UNMANNED UNDERWATER VEHICLE

AHMET KEMAL NENNİOĞLU
MASTER OF SCIENCE

ADANA 2023

REPUBLIC OF TURKEY

ADANA ALPARSLAN TÜRKEŞ SCIENCE AND TECHNOLOGY UNIVERSITY

INSTITUTE OF GRADATE SCHOOL

DEPARTMENT OF MECHANICAL ENGINEERING

DESIGN, MODELLING, AND DYNAMICS SIMULATION OF UNMANNED UNDERWATER VEHICLE

AHMET KEMAL NENNİOĞLU

MASTER OF SCIENCE

SUPERVISOR

ASSIST. PROF. DR. ABDURRAHİM DAL

ADANA 2023

I hereby declare that all information in this thesis has been obtained and presented in accordance with academic rules and ethical conduct. I also declare that, as required by these rules and conduct, I have fully cited and referenced all information that is not original to this work.

[Signature]

Ahmet Kemal NENNİOĞLU

ABSTRACT

DESIGN, MODELLING, AND DYNAMICS SIMULATION OF UNMANNED UNDERWATER VEHICLE

Ahmet Kemal Nennioğlu

Department of Mechanical Engineering
Supervisor: Assist. Prof. Dr. Abdurrahim DAL

August 2023 75 pages

Throughout the ages of the world history, mankind has built civilizations around the water sources such as rivers, lakes, seas, and oceans due to the need of access to lifesources in these water sources. The food sources, natural resources, and biodiversity of the water bodies requires underwater research, as well as military purposes because of ensuring the security of the nations. A small portion of water mass around the earth can be explored by traditional manned water vehicles however in order to obtain full knowledge about water bodies, unmanned underwater vehicle are compulsory to be researched.

In this study, design, modelling, and dynamics simulation of a noval unmanned underwater vehicle is presented. First, status of the unmanned underwater vehicle technology in the literature is shared. Then the geometrical design of the vehicle and structural details are explained. The concept of reference frames, Euler angles and transformation matrices is defined. The kinematic and dynamic models of the vehicle is derived. Using the models, dynamic simulations of the vehicle are carried out. The results of the simulations are discussed and related future work is shared.

Keywords: unmanned underwater vehicle, dynamic simulation, modelling

ÖZET

İNSANSIZ SUALTI ARACININ TASARIMI, MODELLENMESİ VE DİNAMİK SİMULASYONU

Ahmet Kemal NENNİOĞLU
Makine Mühendisliği Anabilim Dalı
Danışman: Dr. Öğr. Üyesi Abdurrahim DAL

Ağustos 2023, 75 sayfa

Dünya tarihinde çağlar boyunca uygarlıklar yaşam kaynaklarına erişim ihtiyacı sebebiyle akarsu, göl, deniz ve okyanus gibi su kaynakları etrafında inşa edilmiştir. Bu su kütlelerindeki gıda kaynakları, doğal kaynaklar, biyolojik çeşitlilik ve toplumların güvenliğinin korunması için askeri amaçlar sualtı araştırmalarını zorunlu kılmıştır. Dünyadaki su kütlesinin küçük bir kısmına geleneksel deniz araçları ile ulaşılabilmektedir fakat tam bilgiye ulaşabilmek için insansız sualtı araçlarının araştırılması zorunludur.

Bu çalışmada özgün bir insansız sualtı aracının tasarımı, modellenmesi ve dinamik simulasyonu sunulmuştur. Öncelikle, insansız sualtı teknolojisinin literatürdeki mevcut durumu paylaşılmış ardından aracın geometrik tasarımı ve yapısal detayları verilmiştir. Koordinat sistemleri, Euler açıları ve dönüşüm matrisleri kavramları tanımlanmıştır. Aracın kinematik ve dinamik modelleri türetilmiş ve bu modeller kullanılarak dinamik simulasyonlar yapılmıştır. Simulasyon sonuçları tartışılmış ve konu ile ilgili planalanan gelecek çalışmalar sunulmuştur.

Anahtar Kelimeler: insansız su altı aracı, dinamik simulasyon, modelleme

To my family

ACKNOWLEDGEMENTS

Firstly, I would like to thank to my advisor, Dr. Abdurrahim DAL for his support for my master study. I am grateful to him for sharing his valuable experience and knowledge and giving me the opportunity to study with him.

Secondly, I would like to thank to my family, my mother Dilek NENNİOĞLU, my father Bekir NENNİOĞLU and my sister Ayşe NENNİOĞLU TURGUT, for their help to become who I am and always being there for me.

Most especially, I would like to express my gratitude to my wife, Gülsüm SARIBOĞA NENNİOĞLU, for her endless support and believing in me.

Last but not the least, my little son Kemal Ege, this is for you.

TABLE OF CONTENTS

CERTIFICATION OF APPROVAL ....**Hata! Yer işareti tanımlanmamış.**
ABSTRACT v
ÖZET vi
ACKNOWLEDGEMENTS viii
TABLE OF CONTENTS ix
LIST OF FIGURES x
LIST OF TABLES xii
LIST OF ABBREVATIONS xiii
LIST OF SYMBOLS xiv
1. INTRODUCTION 15
2. LITERATURE REVIEW 17
3. DESIGN AND STRUCTURE 21
4. KINEMATIC AND DYNAMIC MODELS 23
4.1 Kinematics 23
4.2 Dynamics 29
4.2.1 Rigid Body Dynamics 30
4.2.2 Hydrodynamic Forces and Moments 32
4.2.3 External Forces and Moments 35
5. PARAMETER ESTIMATION AND DYNAMIC SIMULATION 38
5.1 Model Parameters 38
5.1.1 Assumptions 38
5.1.2 Parameters 39
5.2 Dynamic Simulation 43
5.3 Control of the Unmanned Underwater Vehicles 53
5.3.1 Feedback Linearization 53
5.3.2 Reference Tracking 55
5.3.3 Dynamic Simulation with PD Control 56
6. CONCLUSIONS 68
REFERENCES 70

LIST OF FIGURES

Figure 2.1 (a) STARFISH (b) Omni-Egg (c) SUR III (d) ICHTUS (e) AUV-150 19
Figure 3.1 Isometric view of the vehicle 21
Figure 3.2 Required dimensions of the vehicle 22
Figure 4.1 Visualization of the reference frames and DOFs 24
Figure 4.2 Coordinate rotation about z-axis by angle 26
Figure 4.3. Diagram of propeller position for use of mapping matrix 37
Figure 5.1. Two-dimensional added mass coefficient for rectangular cross section 40
Figure 5.2. Infinitesimal analysis for the yaw damping 42
Figure 5.3. Block diagram of the open loop system 44
Figure 5.4. Surge, sway, and heave results of the simulation of first case 45
Figure 5.5. Roll, pitch, and yaw results of the simulation of the first case 45
Figure 5.6. The motion of the first case in 3-D coordinate system 46
Figure 5.7. Surge, sway, and heave results of the simulation of the second case 46
Figure 5.8 Roll, pitch, and yaw results of the simulation of the second case 47
Figure 5.9. The motion of the second case in 3-D coordinate system 47
Figure 5.10. Surge, sway, and heave results of the simulation of the third case 48
Figure 5.11. Roll, pitch, and yaw results of the simulation of the third case 48
Figure 5.12. The motion of the third case in 3-D coordinate system 49
Figure 5.13. Surge, sway, and heave results of the simulation of the fourth case 50
Figure 5.14. Roll, pitch, and yaw results of the simulation of the fourth case 50
Figure 5.15. The motion of the fourth case in 3-D coordinate system 51
Figure 5.16. Surge, sway, and heave results of the simulation of the fifth case 52
Figure 5.17. Roll, pitch, and yaw results of the simulation of the fourth case 52
Figure 5.18. The motion of the fourth case in 3-D coordinate system 53
Figure 5.19. Block diagram of the simulation with PD control 56
Figure 5.20. Surge, sway, and heave results of the simulation of the first case with PD control 57
Figure 5.21. Roll, pitch, and yaw results of the simulation of the first case with PD control. 58
Figure 5.22. The motion of the first case with PD control in 3-D coordinate system 58
Figure 5.23. Surge, sway and heave results of the simulation of the second case with PD control 59
Figure 5.24. Roll, pitch, and yaw results of the simulation of the second case with PD control 59
Figure 5.25. The motion of the second case with PD control in 3-D coordinate system 60
Figure 5.26. Surge, sway and heave results of the simulation of the third case with PD control 60
Figure 5.27. Roll, pitch, and yaw results of the simulation of the third case with PD control 61
Figure 5.28. The motion of the third case with PD control in 3-D coordinate system 61

Figure 5.29. Block diagram of simulation with propeller input 62
Figure 5.30. Surge, sway and heave results of the simulation of the first case with propeller input 63
Figure 5.31. Roll, pitch and yaw results of the simulation of the first case with propeller input 63
Figure 5.32. The motion of the third case with propeller inputs in 3-D coordinate system.... 64
Figure 5.33. Surge, sway and heave results of the simulation of the second case with propeller input 64
Figure 5.34. Roll, pitch and yaw results of the simulation of the second case with propeller input 65
Figure 5.35. The motion of the second case with propeller inputs in 3-D coordinate system 65
Figure 5.36. Surge, sway and heave results of the simulation of the third case with propeller input 66
Figure 5.37. Roll, pitch and yaw results of the simulation of the third case with propeller input 66
Figure 5.38. The motion of the third case with propeller inputs in 3-D coordinate system.... 67

LIST OF TABLES

Table 2.1 AUV Structure Examples 18
Table 4.1 Standard SNAME notations 23
Table 5.1. Propeller inputs of the open loop system 44
Table 5.2. The needed net forces and torques with PD control 62
Table 5.3. Computed propeller inputs 67

LIST OF ABBREVATIONS

AUV	: Autonomous Underwater Vehicle
UUV	: Unmanned Underwater Vehicle
ROV	: Remotely Operated Vehicle
DOF	: Degree of Freedom
SNAME	: Society of Naval Architects and Marine Engineers

LIST OF SYMBOLS

x, y, z	: Linear positions
φ, θ, ψ	: Angular positions
u, v, w	: Linear velocities
p, q, r	: Angular velocities
M_{RB}, M_A	: Rigid body and added mass matrices
C_{RB}, C_A	: Rigid body and added mass Coriolis and centripetal forces matrices
D	: Damping matrix
τ	: Force and torque vector

1. INTRODUCTION

Two thirds of the earth's surface is covered by oceans, seas, lakes, and river, all of which includes food source, natural resources and biodiversity (Shi et al., 2017). Discovery of these elements of water and military purposes led innovators to design underwater vehicles. First known design of an underwater vehicle was produced by English mathematician William Bourne in 1578 however construction of an underwater vehicle is carried out by Dutchman Cornellius Van Drebbel in 1620(Craven et al., 1998). As population grows, the need of exploring these bodies of water increases. Some of the water masses of the earth can be reached by traditional manned marine vehicles however, exploration of large portion of the water, which is still mostly unexplored, by manned vehicles, is either too risky for people or too costly. Thus, unmanned underwater vehicles (UUV) have been investigated since the early 1970s(Kou et al., 2018). Most of the early UUV research was made for military purposes and funded by US Navy. The first nonmilitary uses of UUV started due to discovery of oil and gas masses in North Sea. Early examples of both military and commercial UUV are remotely operated vehicles (ROV) which are still used in offshore industry. However lately autonomous type of UUV is heavily investigated (Vervoort, 2009).

The term UUV includes remotely operated vehicles (ROV) and autonomous underwater vehicles (AUV). The difference between these types of UUV is that ROV are operated by use of a cable or link connected to a platform (mostly a ship). This connection cable supplies energy and required signals which are produced by a human operator. Therefore, ROV do not make their own decisions, i.e., they are not autonomous(El-Hawary, 2000). Whereas AUV includes their own battery to supply energy, sensor systems such as sonar and processors to produce operation signals. They are expected to carry out tasks without a human operator while adapting to environmental elements(Cristi et al., 1990).

In this thesis, design, modelling and dynamics simulation of unmanned underwater vehicle is studied. In Chapter 2, background of the unmanned underwater vehicle technology is reviewed. In Chapter 3, the structure and geometry of the vehicle is presented. In Chapter 4, the kinematic and dynamic model of the unmanned underwater vehicle is introduced. Theoretical concepts such as Euler angles, rotation matrices, reference frames are explained. The dynamic equations are investigated, and an accurate dynamic model is derived. In Chapter 5, parameter estimation and dynamics simulation are conducted. Accurate assumptions are made in order to estimate parameters analytically. Using estimated parameters and MATLAB software a set of simulations carried out. First, the accuracy of the model is tested. Then using control techniques such as feedback linearization and PD control, the vehicle is simulated to follow a constant reference. The results are discussed. In Chapter 6, the study is concluded, and future plans are presented.

2. LITERATURE REVIEW

Application areas of AUV vary over the years. The first main application area is military. Shome et al. developed a modular shallow water vehicle called AUV-150 which can perform military tasks such as surveillance, ocean exploration, bathymetric study, and mapping of the ocean floor. Bluefin Robotics Corporation developed an AUV called Bluefin21 which aims to fulfill the tasks of mine countermeasures, search and rescue, and anti-submarine warfare (Panish & Taylor, 2011) Allotta et al. has launched the ARROWS project which includes different AUV designs one of which is called U-CAT. U-CAT is a highly experimental biomimetic vehicle which performs inspection of wreckage. Prats et al. designed an AUV called GIRONA 500 I-AUV which is a lightweight vehicle with an additional manipulator in order to carry out intervention missions such as air crash investigation and payload delivery to ocean floor. Scientific studies are the second main application area of AUV. Katzschmann et al. developed SoFi, a soft robotic fish which helps to explore underwater life by mimicking a fish and contributes to marine biology field. Tri-TON 2 is a hovering type AUV designed by Sato et al. in order to produce detailed 3D seafloor imaging of Kagoshima Bay, Japan, enabling unmanned geological survey of underwater zones. Two modular AUV, Marta and A-Size, built by Allotta et al. aim to help underwater archeological research. Desa et al. developed Maya AUV which fulfills the environmental monitoring task by use of a camera and other sensors. The final main application area of AUV is industrial needs. SAUVIM of Marani et al. is an AUV with a underwater manipulator which successfully performed a recovery task underwater. Kato developed AE1000 in order to track the deficiency on underwater cables and repair if there is any. SeaCat, which is an AUV designed by Jacobi is capable of detecting the structure underwater such as walls, vessels, rocks etc. Further application areas of AUV can be found it both (Sahoo et al., 2019) and *AUVAC* webpage.

The body structure, i.e., shape of the AUV is very important because of mainly two reasons. The first one is that it needs to keep all mechanical and electronic components inside protecting them from water surroundings. The second reason is that it has part to determine the dynamic equations since shape affects fluid forces such as drag and lift. Early and still most of the designs are torpedo shaped similar to submarines including the first AUV, SPURV(Widditsch, n.d.). These type of AUV are proved to be successful at robust control schemes and empirical formula approximation however have fewer degrees of freedom than the shapes that will be mentioned

(R. Yang et al., 2015). Another popular AUV shape is spherical which offers greater maneuverability in constricted spaces. Also, spherical AUV can perform "zero-radius" turn which enables the vehicle reach points that torpedo shaped ones can not reach(Eldred et al., 2021). Apart from these geometric shapes, researchers have been influenced by underwater animals, namely bio-mimetic AUVs. Advantages of these type of AUV is the ability of mimicking efficiency of animals such as good maneuverability, high deployment time and reliability(Roper et al., 2011). In addition, aquatic life is not disturbed while integrating bio-mimetic AUVs because of their resemblance to underwater animals. Most of the bio-mimetic AUVs are fish robots however in recent studies vehicles mimicking other animals like snake, turtle, crab etc. have been developed. Lately, modular design as a body structure of AUVs have been drawing increasing interest. Modular design breaks the system into several numbers of modules. Modules are configurable if followings are needed: change of mission, fault diagnosis, breakdown or insufficiency of an element (Shome et al., 2012).Several examples in literature are given in Table 1 and can be seen in Figure 1.

Table 2.1 AUV Structure Examples

Body Structure	AUV Name
Torpedo Shaped	STARFISH (Hong et al., 2010)
	Maya (Desa et al., 2007)
	FOLAGA (Alvarez et al., 2005)
	SPARUS II (Carreras et al., 2018)
Egg-shaped	Omni-Egg (Fittery et al., 2012)
Spherical	SUR III (Li et al., 2017)
	WIEVLE (Eldred et al., 2021)
Bio-mimetics	SoFi (Katzschmann et al., 2018)
	ICHTUS (G. H. Yang et al., 2011)
Modular Design	AUV-150 (Shome et al., 2012)
	Bluefin21 (Panish & Taylor, 2011)

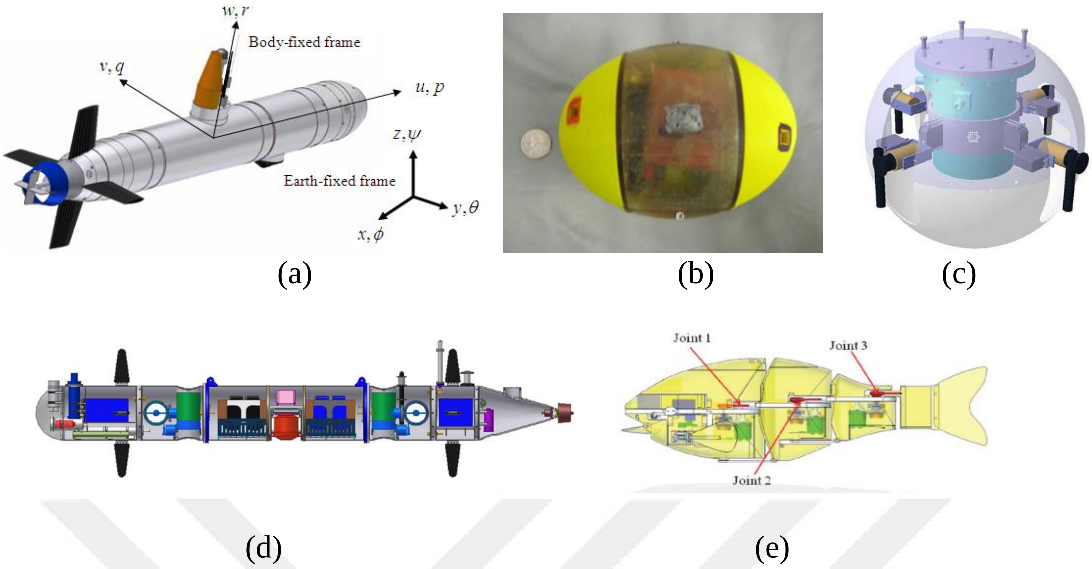

Figure 2.1 (a) STARFISH (b) Omni-Egg (c) SUR III (d) ICHTUS (e) AUV-150

The control of the unmanned underwater vehicles are difficult due to complex nonlinear dynamics, high parametric uncertainties, expensive cost of actuators and sensors, inaccessible states (Tijjani et al., 2022). The nonlinearity of dynamics of the unmanned underwater vehicles are results in multiple-input-multiple-output systems, of which degrees of freedom are coupled(Liu et al., 2019). Even though the nonlinearity is somehow eliminated, the parametric uncertainties makes the control problem extremely challenging(McMahon & Plaku, 2016). During the operation of unmanned underwater vehicles, the need of knowledge and management of states requires advanced sensors and actuators, which are costly(Harris & Whitcomb, 2021). Due to the low performance of these elements of the vehicle, high control effort is needed. Some of the states of the vehicle cannot be known, measured, or analytically estimated, because of technical or economical reasons. The popular solution to this problem in the literature is to employ an observer design(Zemouche et al., 2019). Observers are able to estimate unknown parameters, states, and also, disturbances. Hence, it is a highly popular research topic in order to reduce sensor costs.

The main tasks of the control of unmanned underwater vehicles are path following, station keeping, and trajectory tracking. Path following is the task of the vehicle in which it has to follow a determined path. Station keeping means maintaining the position of the vehicle.

Trajectory tracking is the mission of the vehicle keeping track of a time-varied trajectory. There are many control techniques used for unmanned underwater vehicle, but most favored ones can be listed as PD/PID control, sliding mode control, adaptive control, and observation-based control. PD/PID control is also known as classical control laws. It includes feedback gains from the error in a defined reference to the input. It is commonly used in researches due to the simplicity of design and implementation (Gan et al., 2020). PD/PID control suffers from inability of obtaining a high accuracy dynamic model due to hydrodynamic effects (Zhu & Sun, 2013). However, the reason of being common in the literature is the comprehensive knowledge and therefore the usage of comparison with advanced control techniques(Zhao & Guo, 2021). Uncertain parameters and disturbances leads the researches of unmanned underwater vehicles to the design of a robust control schemes(Bejarbaneh et al., 2020). A popular of the such techniques are slide mode control, the idea behind which is that the control law signal is discontinuous, helps to converge to adjacent region, and takes a different form(Hu et al., 2020)(Ahmad et al., 2020). Although sliding mode control can overcome the parametric uncertainties, it needs the boundaries of uncertainties, in other words, an interval of parameters, which is usually difficult to obtain. In the cases the defined feedback gains for corresponding parameter intervals are failed in critical hydrodynamic conditions, the literature offers auto adjusting the control gains which is called adaptive control(Zhang et al., 2022). Despite being a toilsome process, adaptive control presents many solutions to control problems of unmanned underwater vehicles. The literature usually strongly assume that all states of the vehicle are known or measurable in order to implement previously mentioned control techniques. However, in practice most of the states of an unmanned underwater vehicle are inaccessible(Baruch et al., 2020). Thus, there are much research in the literature focusing on the design of an observer which helps to estimate the states of the vehicle. Observer design also a solution to expensive cost of sensors. It should be noted, the viable choice of designing an unmanned underwater vehicle is the employment of combined technique of using above strategies for compatible tasks. While achieving stability and robustness, computational heaviness must be avoided as possible.

3. DESIGN AND STRUCTURE

The AUV which will be studied in this thesis is designed by the help of Adana Alparlsan Türkeş Science and Technology University bachelor students. It is designed in SolidWorks and aimed to be available for 3D printing. In order to enable easier movement underwater and being more suitable to hydrodynamics, the cross-section area widens from the front to the middle and narrows from the middle to the rear. Isometric view is given in Figure 3.1

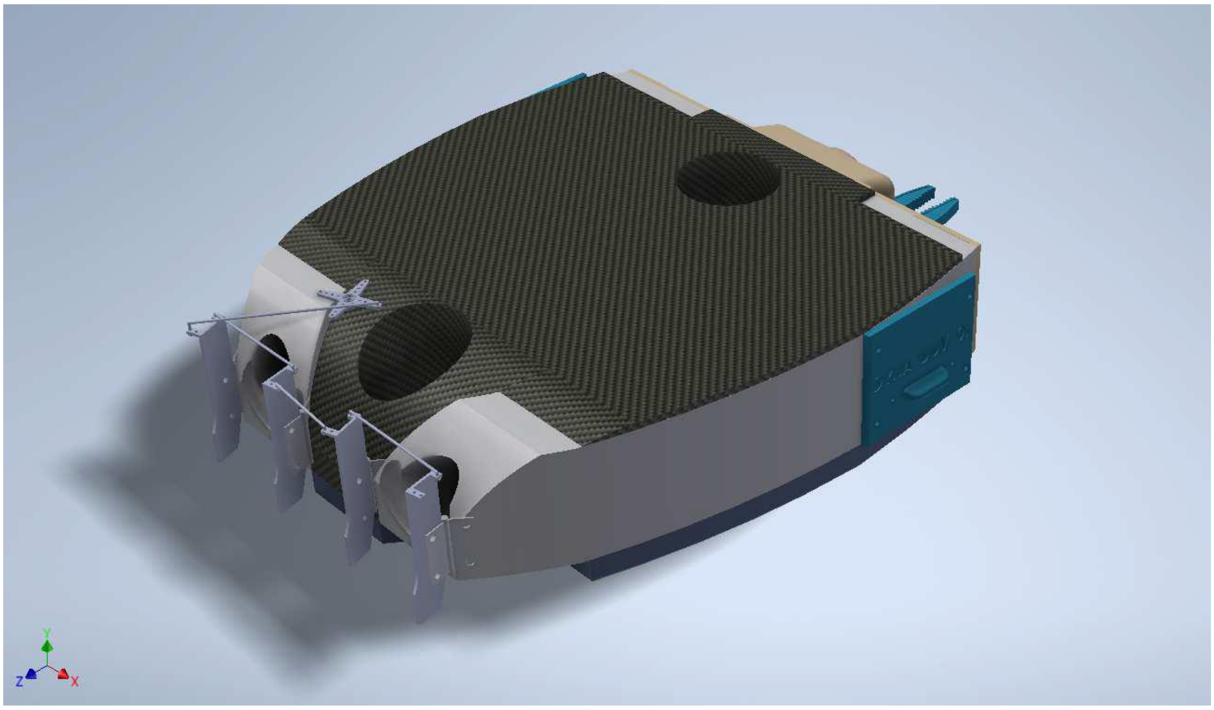

Figure 3.1 Isometric view of the vehicle

The vehicle runs with four propellers, two of which are for horizontal movement and maneuver and the other two are for vertical movement. When the left propeller on the rear of the vehicle works, the vehicle will head to the right, and when the right propeller works, the vehicle will head to the left. In order to derive the moment effect of the rear propellers the position with respect to the vehicle must be known. The dimension of the vehicle and positions of the propellers in millimeters is given in Figure 3.2. Here the effect of the propellers will be assumed to be point forces at the middle point of propellers. SolidWorks data for mass or inertia of the vehicle will be used when needed.

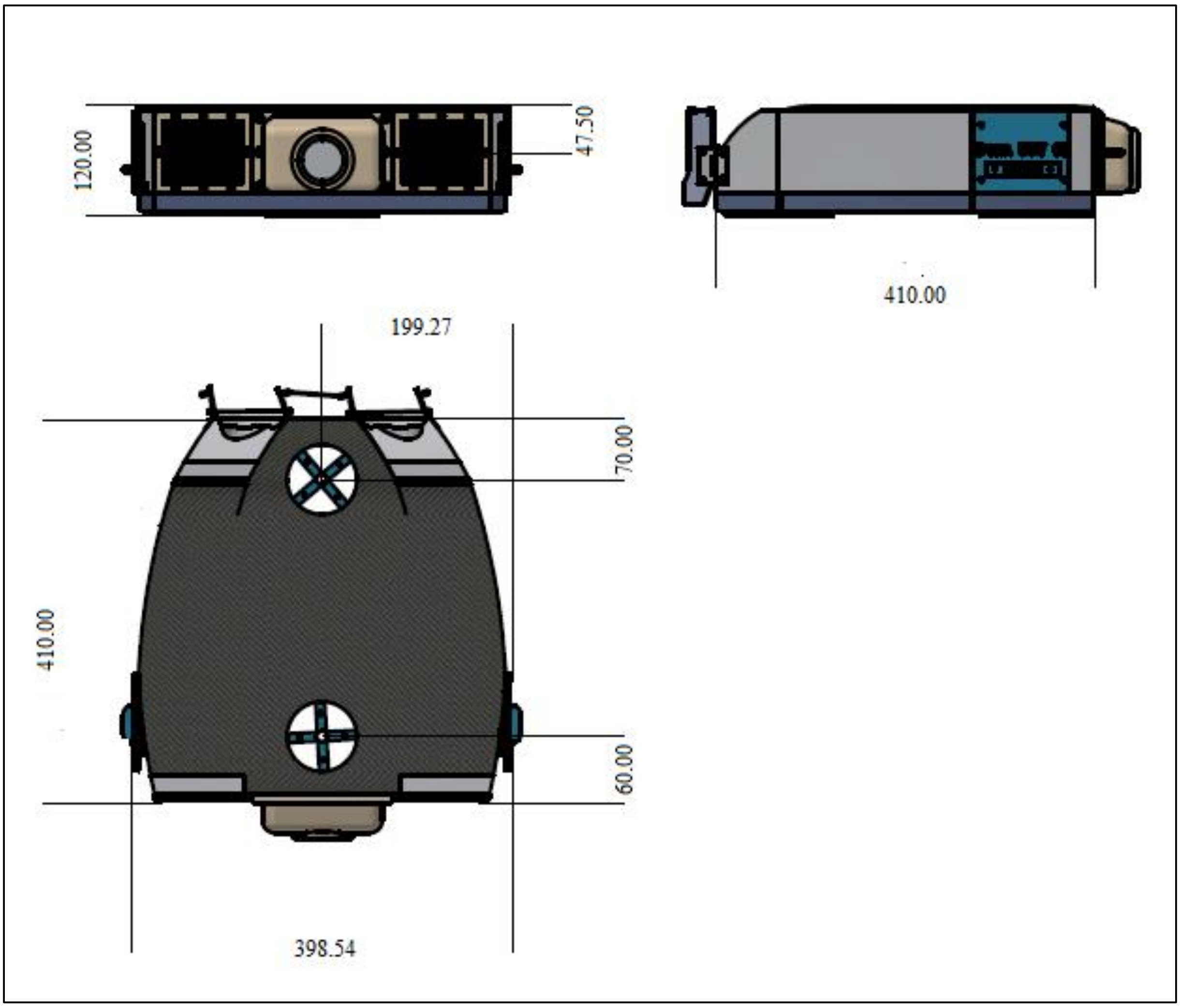

Figure 3.2 Required dimensions of the vehicle

4. KINEMATIC AND DYNAMIC MODELS

The environment in which underwater vehicles operate makes the control of AUVs more difficult because of the multiple complex and non-linear forces acting on them. These forces can be exemplified as hydrodynamic drag, damping, lift forces, Coriolis and centripetal forces, gravity and buoyancy forces, and also unknown environmental disturbances. All of the forces must be calculated, measured, or estimated in order to include in dynamic model. Further study regarding these forces will be done in following chapters. This chapter focuses on derivation of kinematic and dynamic model of the vehicle. Section 4.1 introduces the kinematics of a 6-DOF unmanned underwater vehicle. The concepts of Euler angles, rotation matrices and reference frames are presented. Section 4.2 studies the dynamics of the vehicle. The equation of motion is presented and its terms explained.

4.1. Kinematics

Kinematics includes, by definition, the position, orientation, velocity, acceleration, and further higher-order derivatives of a body. The term does not investigate force and torque of the body which will be revisited in following sections (Siciliano & Khatib, 2008). Kinematics is the first step and most fundamental aspect of design, analysis, simulation, and control of the devices and vehicles such as robots, drones, and unmanned vehicles. In order to complete following procedures of the AUV design, kinematic model of the AUV will be introduced in this section. The techniques and methods are the reference frames, the Euler angles, and state space representation.

Table 4.1 Standard SNAME notations

DOF	Motion Descriptions	Positions and Orientations	Linear and Angular Velocities
1	Motions in the X- direction (surge)	x	u
2	Motions in the Y- direction (sway)	y	v
3	Motions in the Z- direction (heave)	z	w
4	Rotations about the X-axis (roll)	φ	p
5	Rotations about the Y-axis (pitch)	θ	q
6	Rotations about the Z-axis (yaw)	ψ	r

According to Society of Naval Architects and Marine Engineers (SNAME), there are six degrees of freedom which are namely surge, sway, heave, roll, pitch and yaw(SNAME, 1950). Descriptions and notation of these are presented in Table 2. Two reference frames are introduced in order to describe the position, orientation, velocity, and acceleration of the vehicle. First is the earth fixed reference frame with the origin O_0 of which x, y and z axes are directed to the north, east and the center of the world, respectively. Second is body fixed reference frame with the origin O_B of which x, y and z axes are directed to forward direction, right of the vehicle and down vertically, respectively. In Figure 2 the two reference frames and related degrees of freedom can be seen.

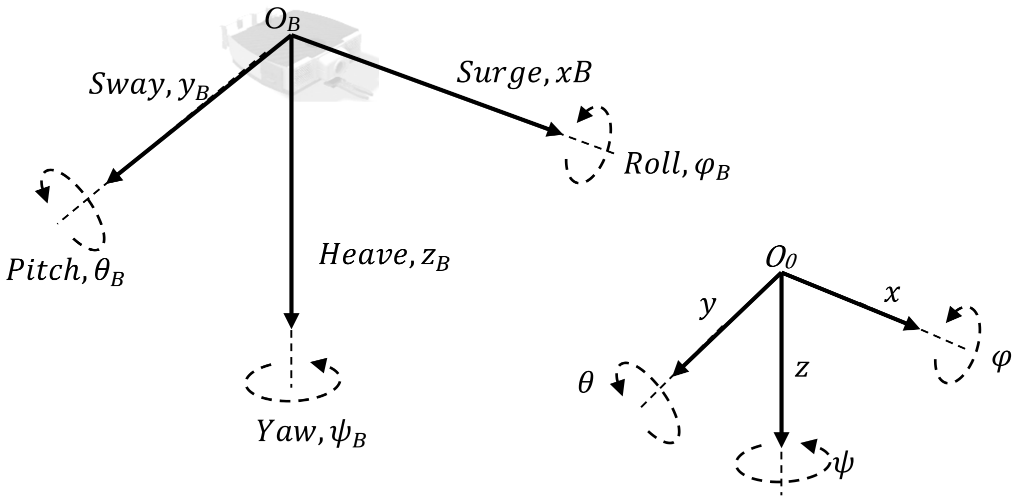

Figure 4.1 Visualization of the reference frames and DOFs

The degrees of freedom, i.e. positions and orientations with respect to earth fixed frame and body fixed frame are notated as X and η and their vector forms are given below.

$$X = [\, surge\ sway\ heave\ roll\ pitch\ yaw \,]^T$$
$$= [x_B\ y_B\ z_B\ \varphi_B\ \theta_B\ \psi_B] \quad (4.1)$$
$$\boldsymbol{\eta} = [\ \mathbf{x}\ \ \mathbf{y}\ \ \mathbf{z}\ \ \boldsymbol{\Phi}\ \ \boldsymbol{\theta}\ \ \boldsymbol{\psi}\ ]^{\mathbf{T}} \quad (4.2)$$

With the help of body fixed and earth fixed reference frames velocity and acceleration of the vehicle with respect to body and earth can be determined. Also, orientation of the vehicle with respect to earth can be determined.

The two reference frames are related to each other with help of Euler angles. In order to make use of Euler angles, the concept of the rotation matrices must be studied. A rotation matrix is a matrix which rotates a vector by a certain angle while keeping the length same. The rotation matrices which are used for Euler angles are notated by *R*, and hold following(Diebel, 2006):

- $R \in SO(3)$: special orthogonal group of all 3×3 rotational matrices
- $\det R = \pm 1$ and $R^{-1} = R^T$
- $\mathbf{z'} = R\mathbf{z}$ and $\mathbf{z} = R^T\mathbf{z'}$

Coordinate rotation is another concept which should be mentioned to fully employ Euler angles. It can be defined as the rotation about a single coordinate axis. Notations for *x*-, *y*-, *and z*-axes are R_1, R_2, and R_3, respectively. $R_i : \mathbb{R} \rightarrow SO(3)$ for $i \in \{1,2,3\}$ are given below.

$$R_1(\alpha) = \begin{bmatrix} 1 & 0 & 0 \\ 0 & cos(\alpha) & sin(\alpha) \\ 0 & -sin(\alpha) & cos(\alpha) \end{bmatrix} \tag{4.3}$$

$$R_2(\alpha) = \begin{bmatrix} cos(\alpha) & 0 & -sin(\alpha) \\ 0 & 1 & 0 \\ sin(\alpha) & 0 & cos(\alpha) \end{bmatrix} \tag{4.4}$$

$$R_3(\alpha) = \begin{bmatrix} cos(\alpha) & sin(\alpha) & 0 \\ -sin(\alpha) & cos(\alpha) & 0 \\ 0 & 0 & 1 \end{bmatrix} \tag{4.5}$$

These rotation matrices are multiplied with different sequences of three (Euler angle sequences) to form the rotation from one frame to another. A rotation matrix is also derived from a different point of view called direction cosine matrix, which can be defined as a 3×3 matrix elements of which consist of cosines of the angles between all axes of the two frames at corresponding positions. In the case of earth fixed and body fixed frames with the axes (x, y, z) and (*x', y', z'*) respectively, direction cosine matrix takes the form of following;

$$\boldsymbol{R} = \begin{bmatrix} \boldsymbol{cos(\theta_{x'x})} & \boldsymbol{cos(\theta_{x'y})} & \boldsymbol{cos(\theta_{x'z})} \\ \boldsymbol{cos(\theta_{y'x})} & \boldsymbol{cos(\theta_{y'y})} & \boldsymbol{cos(\theta_{y'z})} \\ \boldsymbol{cos(\theta_{z'x})} & \boldsymbol{cos(\theta_{z'y})} & \boldsymbol{cos(\theta_{z'z})} \end{bmatrix} \tag{4.6}$$

where $\theta_{x'y}$ is, for example, the angle between x'-axis and y-axis. Note that every combination of all three axis of two different frames is included in the above matrix.

In order to visualize the two concepts mentioned above, namely coordinate rotation and direction cosine matrix, consider the case shown in Figure 3, which is simply a rotation about z-axis.

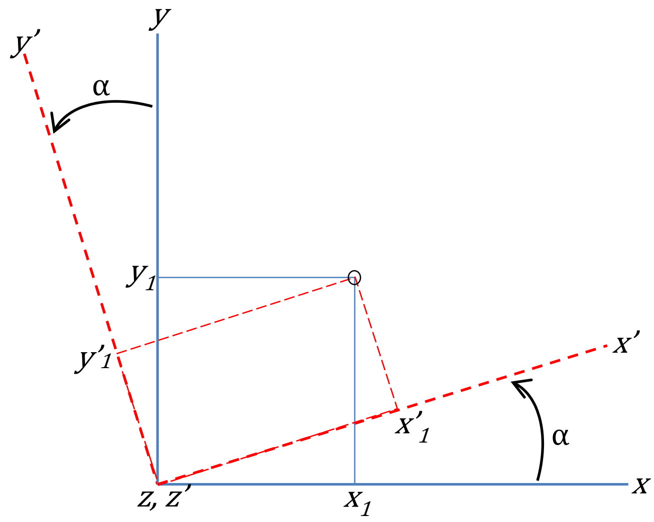

Figure 4.2 Coordinate rotation about z-axis by angle

Applying the equation 4.6 for the case in figure 3, the equation takes the form below.

$$\boldsymbol{R} = \begin{bmatrix} \cos(\alpha) & \cos(\frac{\pi}{2} - \alpha) & 0 \\ \cos(\frac{\pi}{2} + \alpha) & \cos(\alpha) & 0 \\ 0 & 0 & 1 \end{bmatrix}$$

$$= \begin{bmatrix} \cos(\alpha) & \sin\alpha & 0 \\ -\sin\alpha & \cos(\alpha) & 0 \\ 0 & 0 & 1 \end{bmatrix} \tag{4.7}$$

As expected, equations 4.5 and 4.7 are the same. As mentioned above, multiplication of rotation matrices given in equations 4.3-5 is named Euler angle sequences which consist of twelve possible sets (Pio, 1966).These sets are named according to their sequence of rotation about corresponding axis as can be formulated as below.

$$\boldsymbol{R_{ijk}(\varphi, \theta, \psi) = R_i(\varphi) R_j(\theta) R_k(\psi)} \tag{4.8}$$

where above equation is notated as i-j-k Euler sequence. Most common choices of Euler sequences in the literature are 3-1-3, 3-2-3 and 3-2-1. Among these choices 3-2-1 is the most used one in naval and aerospace applications. Therefore, in this study, 3-2-1 Euler sequence will be used. In order to obtain a rotation matrix aligning a vector in a body-fixed frame to earth-fixed frame rotation matrices in order of equation 4.5, 4.4, 4.3 are multiplied as shown below.

$$R_{321}(\psi,\theta,\varphi) = R_3(\psi)R_2(\theta)R_1(\varphi)$$

$$R_{321}(\psi,\theta,\varphi) = \begin{bmatrix} C(\psi) & S(\psi) & 0 \\ -S(\psi) & C(\psi) & 0 \\ 0 & 0 & 1 \end{bmatrix} \begin{bmatrix} C(\theta) & 0 & -S(\theta) \\ 0 & 1 & 0 \\ S(\theta) & 0 & C(\theta) \end{bmatrix} \begin{bmatrix} 1 & 0 & 0 \\ 0 & C(\varphi) & S(\varphi) \\ 0 & -S(\varphi) & C(\varphi) \end{bmatrix}$$

$$= \begin{bmatrix} C(\theta)C(\psi) & -C(\varphi)S(\psi) + S(\varphi)S(\theta)C(\psi) & S(\varphi)S(\psi) + C(\varphi)S(\theta)C(\psi) \\ C(\theta)S(\psi) & C(\varphi)C(\psi) + S(\varphi)S(\theta)S(\psi) & -S(\varphi)C(\psi) + C(\varphi)S(\theta)S(\psi) \\ -S(\theta) & S(\varphi)C(\theta) & C(\varphi)C(\theta) \end{bmatrix} \tag{4.9}$$

For a compact notation sin and cos functions are notated as S and C respectively. This rotation matrix means that a vector in a body-fixed frame rotated around in turn of *z*-axis, *y*-axis, and *x*-axis. Recalling the position vectors in both body and earth-fixed frames, X and η, in equations 4.1 and 4.2, now we define velocity vectors, v and $\dot{\eta}$, in body and earth-fixed frames respectively and also force/torque vector of thruster input, which will be used in dynamic modelling.

$$\nu = [\ \dot{x}_B\ \ \dot{y}_B\ \ \dot{z}_B\ \ \dot{\varphi}_B\ \ \dot{\theta}_B\ \ \dot{\psi}_B\ ]^T = [\,u\ \ v\ \ w\ \ p\ \ q\ \ r\,]^T \tag{4.10}$$

$$\dot{\eta} = [\ \dot{x}\quad \dot{y}\quad \dot{z}\quad \dot{\varphi}\quad \dot{\theta}\quad \dot{\psi}\,]^T \tag{4.11}$$

$$\tau = \left[\tau_x\ \ \tau_y\ \ \tau_z\ \ \tau_\Phi\ \ \tau_\theta\ \ \tau_\psi\right] \tag{4.12}$$

Position of the vehicle in the body and earth-fixed frames do not differ and described relative to an initial position. One important kinematic feature of the vehicle that is different in body and earth-fixed frame is its orientation. In other words, surge, sway, and heave degrees of freedom are the same for origins of body and earth-fixed frame, however roll, pitch, and yaw degrees of freedom can be different. By definition, earth-fixed frame has the orientation of earth magnetic field, and the orientation of body-fixed frame is described by the direction to which the vehicle is pointed at. The relative orientation of the body-fixed frame to earth-fixed frame is important to know, since this information consists of three angle values which will be used in rotation matrix in equation 4.9, when needed.

The velocity vectors in equation 4.10 and 4.11 includes linear and angular velocities, first three terms and last three terms respectively. The velocity vector transformation from body-fixed frame into earth-fixed frame formulated as below.

$$\dot{\boldsymbol{\eta}} = \boldsymbol{J}(\boldsymbol{\eta})\boldsymbol{\nu} \tag{4.13}$$

where, $\dot{\boldsymbol{\eta}}$ is velocity in earth-fixed frame, $\boldsymbol{\nu}$ is velocity in body-fixed frame, $\boldsymbol{J}(\boldsymbol{\eta})$ is the coordinate transform matrix, and also

$$\dot{\eta} = [\ v_E \ \ \omega_E\ ]^T \tag{4.14}$$

$$\nu = [\ v_B \ \ \omega_B\ ]^T \tag{4.15}$$

$$J(\eta) = \begin{bmatrix} J_1(v_E) & 0 \\ 0 & J_2(\omega_E) \end{bmatrix} \tag{4.16}$$

where v_E and ω_E are linear and angular velocities in earth-fixed frame respectively. v_B and ω_B are linear and angular velocities in body-fixed frame respectively. The coordinate transform matrix $J(\eta)$ consists of two parts for linear and angular velocities. The linear velocity in earth-fixed frame can be found with help of those in body-fixed frame.

$$v_E = J_1(v_E)\, v_B \tag{4.17}$$

where $J_1(v_E) = R_{321}(v_E)$ which is given in equation 4.9. The angular velocity in earth-fixed frame is calculated by using the other coordinate transform matrix, $J_2(\omega_E)$, which, however, calculated in a more complex way.

$$\boldsymbol{\omega_E} = \boldsymbol{J_2}(\boldsymbol{\omega_E})\, \boldsymbol{\omega_B} \tag{4.18}$$

$$\omega_B = {J_2}^{-1}\, \omega_E \tag{4.19}$$

$$\omega_B = \begin{bmatrix} \dot{\varphi} \\ 0 \\ 0 \end{bmatrix} + R_1(\varphi) \begin{bmatrix} 0 \\ \dot{\theta} \\ 0 \end{bmatrix} + R_1(\varphi) R_2(\theta) \begin{bmatrix} 0 \\ 0 \\ \dot{\psi} \end{bmatrix} \tag{4.20}$$

$$\omega_B = \begin{bmatrix} \dot{\varphi} \\ 0 \\ 0 \end{bmatrix} + \begin{bmatrix} 0 \\ \dot{\theta}C(\varphi) \\ -\dot{\theta}S(\varphi) \end{bmatrix} + \begin{bmatrix} \dot{\psi}S(\theta) \\ \dot{\psi}S(\varphi)C(\theta) \\ \dot{\psi}C(\varphi)C(\theta) \end{bmatrix} \tag{4.21}$$

$$\omega_B = \begin{bmatrix} 1 & 0 & -S(\theta) \\ 0 & C(\varphi) & S(\varphi)C(\theta) \\ 0 & -S(\varphi) & C(\varphi)C(\theta) \end{bmatrix} \begin{bmatrix} \dot{\varphi} \\ \dot{\theta} \\ \dot{\psi} \end{bmatrix} \tag{4.20}$$

where $[\,\dot{\varphi} \quad \dot{\theta} \quad \dot{\psi}\,]^T$ is ω_E, thus ${J_2}^{-1} = \begin{bmatrix} 1 & 0 & -S(\theta) \\ 0 & C(\varphi) & S(\varphi)C(\theta) \\ 0 & -S(\varphi) & C(\varphi)C(\theta) \end{bmatrix}$. Taking inverse matrix,

$$J_2(\omega_E) = \begin{bmatrix} 1 & S(\varphi)T(\theta) & C(\varphi)T(\theta) \\ 0 & C(\varphi) & -S(\varphi) \\ 0 & S(\varphi)/C(\theta) & C(\varphi)/C(\theta) \end{bmatrix} \tag{4.21}$$

where sine, cosine and tangent functions are denoted as S, C, and T respectively. Due to the tangent function in this coordinate transform matrix, $\boldsymbol{J_2}$ is undefined if $\boldsymbol{\theta} = \pm\frac{\boldsymbol{\pi}}{\mathbf{2}}$. In future applications, pitch values should be carefully observed.

4.2. Dynamics

The dynamic model of a UUV must be accurate for precise control and navigation. The dynamic equation below is derived from Newton-Euler equation of a rigid body in fluid (Fossen, 1994).

$$\boldsymbol{M\dot{\nu}} + \boldsymbol{C}(\boldsymbol{\nu})\boldsymbol{\nu} + \boldsymbol{D}(\boldsymbol{\nu})\boldsymbol{\nu} + \boldsymbol{g}(\boldsymbol{\eta}) = \boldsymbol{\tau} \tag{4.22}$$

where $M = M_{RB} + M_A$; M_{RB} and M_A are the constant inertia and added mass matrix of the AUV respectively, $C(\nu) = C_{RB}(\nu) + C_A(\nu)$; $C_{RB}(\nu)$ and $C_A(\nu)$ are the Coriolis and centripetal matrix of the rigid body, and the added mass respectively, $\mathbf{D}(\boldsymbol{\nu})$ is the damping matrix containing drag and lift terms, $\mathbf{g}(\boldsymbol{\eta})$ is the vector of restoring forces and moments which includes gravitational and buoyancy forces, and $\boldsymbol{\tau}$ is the vector of body-fixed forces from the actuators. Environmental disturbances such as underwater currents are neglected in this equation.

The parameters in the equation 4.22 should be analyzed in two parts, rigid body dynamics and hydrodynamic forces/moments since the components M_{RB} and C_{RB} are strictly related to dynamics of rigid body, and the remaining components such as C_{RB}, C_A, and **D** are related to the hydrodynamic effects.

4.2.1. Rigid Body Dynamics

Rigid body dynamics which exclude the hydrodynamic effects of the water to vehicle is given in the below equation in a compact form.

$$M_{RB}\dot{\nu} + C_{RB}(\nu)\nu = \tau_{RB} \tag{4.23}$$

The explicit form of the equation 4.23 is given as below.

$$m\dot{v} + m\dot{\omega} \times r_G + m\omega \times v + m\omega \times (\omega \times r_G) = F_{RB} \tag{4.24}$$

$$I_B\dot{\omega} + \omega \times (I_B\omega) + mr_G \times \dot{v} + mr_G \times (\omega \times v) = Q_{RB} \tag{4.25}$$

where m is mass of the vehicle, I_B is the inertia tensor with respect to body-fixed frame which is

$$I_B = \begin{bmatrix} I_{xx} & -I_{xy} & -I_{xz} \\ -I_{yx} & I_{yy} & -I_{yz} \\ -I_{zx} & -I_{zy} & -I_{zz} \end{bmatrix} \tag{4.26}$$

$r_G = [x_G\, y_G\, z_G]^T$ is the center of gravity with respect to body-fixed frame, and F_{RB} and Q_{RB} are the external force and torque applied to the system, respectively.

In the equations 4.24 and 4.25, the terms multiplied with time derivatives of linear velocity v and angular velocity ω, forms the inertia matrix, M_{RB}. Thus, the term $M_{RB}\dot{\nu}$ in equation 18 can be written as below.

$$M_{RB}\dot{\nu} = \begin{bmatrix} m\dot{v} + m\dot{\omega} \times r_G \\ I_B\dot{\omega} + mr_G \times \dot{v} \end{bmatrix} \tag{4.27}$$

provided that $\nu = [v\ \omega]^T$, M_{RB} can be extracted from above equation

$$M_{RB} = \begin{bmatrix} mI_{3\times3} & -mS(r_G) \\ mS(r_G) & I_B \end{bmatrix} \tag{4.28}$$

where $S(\lambda)$ is, very helpful way of taking cross products of vectors, skew-symmetric matrix operator of a vector $\lambda = \left[\lambda_x \; \lambda_y \; \lambda_z\right]^T \epsilon \; \mathbb{R}^3$, given by

$$S(\lambda) = \begin{bmatrix} 0 & -\lambda_z & \lambda_y \\ \lambda_z & 0 & -\lambda_x \\ -\lambda_y & \lambda_x & 0 \end{bmatrix} \tag{4.29}$$

$$M_{RB} = \begin{bmatrix} m & 0 & 0 & 0 & mz_G & -my_G \\ 0 & m & 0 & -mz_G & 0 & mx_G \\ 0 & 0 & m & my_G & -mx_G & 0 \\ 0 & -mz_G & my_G & I_{xx} & -I_{xy} & -I_{xz} \\ mz_G & 0 & -mx_G & -I_{yx} & I_{yy} & -I_{yz} \\ -my_G & mx_G & 0 & -I_{zx} & -I_{zy} & I_{zz} \end{bmatrix} \tag{4.30}$$

If the origin of the body-fixed frame is placed at the center of gravity of the vehicle, the vector r_G becomes a zero vector and the vehicle assumed the be symmetric in all planes, off-diagonal elements of I_K, i.e., products of inertia, become zero. Hence, we can simplify the inertia matrix M_{RB} as follows

$$M_{RB} = \begin{bmatrix} m & 0 & 0 & 0 & 0 & 0 \\ 0 & m & 0 & 0 & 0 & 0 \\ 0 & 0 & m & 0 & 0 & 0 \\ 0 & 0 & 0 & I_{xx} & 0 & 0 \\ 0 & 0 & 0 & 0 & I_{yy} & 0 \\ 0 & 0 & 0 & 0 & 0 & I_{zz} \end{bmatrix} \tag{4.31}$$

The term $C_{RB}\nu$ in equation 4.23, which can be written with the remaining terms in equation 4.24 and 4.25, is given below.

$$C_{RB}\nu = \begin{bmatrix} m\omega \times v + m\omega \times (\omega \times r_G) \\ \omega \times (I_B\omega) + mr_G \times (\omega \times v) \end{bmatrix} \tag{4.32}$$

Coriolis and centripetal matrix of the rigid body, C_{RB} , can be derived similar to rigid body mass matrix, M_{RB}. After the assumptions made above, C_{RB} simplifies a skew-symmetric matrix as given below.

$$C_{RB} = \begin{bmatrix} 0_{3\times3} & -mS(\mathrm{v}) \\ -mS(\mathrm{v}) & -S(\hat{I}_B\omega) \end{bmatrix}$$
$$= \begin{bmatrix} 0 & 0 & 0 & 0 & m\omega & -mv \\ 0 & 0 & 0 & -m\omega & 0 & mu \\ 0 & 0 & 0 & mv & -mu & 0 \\ 0 & -m\omega & mv & 0 & I_{zz}r & -I_{yy}q \\ m\omega & 0 & -mu & -I_{zz}r & 0 & I_{xx}p \\ -mv & mu & 0 & I_{yy}q & -I_{xx}p & 0 \end{bmatrix} \tag{4.33}$$

Where $\hat{I}_B = diag\{I_B\} \cong I_B$. The complete derivation and proof can be found in (Fossen, 1994). Another parametrization of C_{RB} is given below.

$$C_{RB} = \begin{bmatrix} 0_{3\times3} & -S(M_{11}v + M_{12}\omega) \\ -S(M_{11}v + M_{12}\omega) & -S(M_{21}v + M_{22}\omega) \end{bmatrix} \tag{4.34}$$

Where M_{ik} terms are 3x3 matrices in M_{RB} such as,

$$M_{RB} = \begin{bmatrix} M_{11} & M_{12} \\ M_{21} & M_{22} \end{bmatrix} \tag{4.35}$$

This form of C_{RB} will be helpful later on when deriving hydrodynamic terms.

4.2.2. Hydrodynamic Forces and Moments

Combining equations 4.22 and 4.23, τ_{RB} can be written as following, with the hydrodynamic added terms.

$$\tau_{RB} = \tau - M_A\dot{v} - C_A(v)v - D(v)v - g(\eta) \tag{4.36}$$

Where τ is the force and torque applied by thrusters, M_A and C_A are the hydrodynamic added mass and Coriolis matrices respectively, D is the hydrodynamic damping and lift matrix, and g is the vector of restoring forces and moments which includes gravitational and buoyancy forces.

Using the SNAME notation, M_A is defined as below(SNAME, 1950b).

$$M_A = -\begin{bmatrix} X_{\dot{u}} & X_{\dot{v}} & X_{\dot{w}} & X_{\dot{p}} & X_{\dot{q}} & X_{\dot{r}} \\ Y_{\dot{u}} & Y_{\dot{v}} & Y_{\dot{w}} & Y_{\dot{p}} & Y_{\dot{q}} & Y_{\dot{r}} \\ Z_{\dot{u}} & Z_{\dot{v}} & Z_{\dot{w}} & Z_{\dot{p}} & Z_{\dot{q}} & Z_{\dot{r}} \\ K_{\dot{u}} & K_{\dot{v}} & K_{\dot{w}} & K_{\dot{p}} & K_{\dot{q}} & K_{\dot{r}} \\ M_{\dot{u}} & M_{\dot{v}} & M_{\dot{w}} & M_{\dot{p}} & M_{\dot{q}} & M_{\dot{r}} \\ N_{\dot{u}} & N_{\dot{v}} & N_{\dot{w}} & N_{\dot{p}} & N_{\dot{q}} & N_{\dot{r}} \end{bmatrix} \tag{4.37}$$

Where X, Y, Z are the forces, K, L, M are the torques, and $\dot{u}, \dot{v}, \dot{w}$ are the linear accelerations, and $\dot{p}, \dot{q}, \dot{r}$ are the angular acceleration in x, y, z directions, respectively, and $X_{\dot{u}} = \frac{\partial X}{\partial \dot{u}}$, etc. The terms of hydrodynamic added mass matrix are strictly related to the shape of the vehicle but due to the symmetry assumption, only diagonal terms of M_A can be used. Also, when the vehicle is completely under water, these terms can be assumed constant. Thus, $M_A > 0$ and $\dot{M}_A = 0$.

$$M_A = -\begin{bmatrix} X_{\dot{u}} & 0 & 0 & 0 & 0 & 0 \\ 0 & Y_{\dot{v}} & 0 & 0 & 0 & 0 \\ 0 & 0 & Z_{\dot{w}} & 0 & 0 & 0 \\ 0 & 0 & 0 & K_{\dot{p}} & 0 & 0 \\ 0 & 0 & 0 & 0 & M_{\dot{q}} & 0 \\ 0 & 0 & 0 & 0 & 0 & N_{\dot{r}} \end{bmatrix} \tag{4.38}$$

The hydrodynamic added Coriolis matrix can be derived similar to derivation of rigid body Coriolis matrix in equations 4.34 and 4.35. By rewriting equation 4.38 as below where A_{ik} terms are 3x3 matrices in M_A

$$M_A = \begin{bmatrix} A_{11} & A_{12} \\ A_{21} & A_{22} \end{bmatrix} \tag{4.39}$$

and

$$C_A = \begin{bmatrix} 0_{3\times3} & -S(A_{11}v + A_{12}\omega) \\ -S(A_{11}v + A_{12}\omega) & -S(A_{21}v + A_{22}\omega) \end{bmatrix} \tag{4.40}$$

C_A becomes.

$$C_A = \begin{bmatrix} 0 & 0 & 0 & 0 & -Z_{\dot{w}}w & Y_{\dot{v}}v \\ 0 & 0 & 0 & Z_{\dot{w}} & 0 & -X_{\dot{u}}u \\ 0 & 0 & 0 & -Y_{\dot{v}}v & X_{\dot{u}}u & 0 \\ 0 & -Z_{\dot{w}}w & Y_{\dot{v}}v & 0 & -N_{\dot{r}}r & M_{\dot{q}}q \\ Z_{\dot{w}}w & 0 & -X_{\dot{u}}u & N_{\dot{r}}r & 0 & -K_{\dot{p}}p \\ -Y_{\dot{v}}v & X_{\dot{u}}u & 0 & -M_{\dot{q}}q & K_{\dot{p}}p & 0 \end{bmatrix} \tag{4.41}$$

The damping matrix, $D(v)$ includes all other hydrodynamic forces and moments which are mainly reduced to four parts, potential damping D_P, skin friction D_S, wave drift damping D_W, and vortex shedding damping D_M (R. Yang et al., 2015). D_P and D_W have significant effect on surface vehicles however the contribution of these two in underwater vehicles are negligibly small compared to other damping effects. Therefore, damping matrix is left with two terms and can be expressed as $D(v) = D_S + D_M$. The derivation of damping matrix is quite complex however, non-diagonal terms can be eliminated due to the symmetry assumption and higher order terms can be neglected. Consequently, the damping matrix is reduced to linear and quadratic terms and can be written as $D(v) = D_l + D_q$. The elements of D_l are X_u, Y_v etc. In order to derive the elements of D_q, the axial viscous damping force must be introduced.

$$f(U) = -\frac{1}{2}\rho C_D A U|U| \tag{4.42}$$

where ρ is the density of the fluid, C_D is the damping coefficient which is a function of Reynolds number, A is the cross-sectional area of the vehicle and U is the velocity of the vehicle. The combined damping matrix $D(v)$ is given by

$$D(v) = \begin{bmatrix} X_u + X_{u|u|}|u| & 0 & 0 & 0 & 0 & 0 \\ 0 & Y_v + Y_{v|v|}|v| & 0 & 0 & 0 & 0 \\ 0 & 0 & Z_w + Z_{w|w|}|w| & 0 & 0 & 0 \\ 0 & 0 & 0 & K_p + K_{p|p|}|p| & 0 & 0 \\ 0 & 0 & 0 & 0 & M_q + M_{q|q|}|q| & 0 \\ 0 & 0 & 0 & 0 & 0 & N_r X_{r|r|}|r| \end{bmatrix} \tag{4.43}$$

where , $X_{u|u|} = \frac{\partial X}{\partial(u|u|)} = -\frac{1}{2}\rho C_D A$ and X is the axial viscous damping force as in equation 4.42, in respective direction.

4.2.3. External Forces and Moments

External forces are the remaining terms in equation in 4.22. They include gravitational and buoyancy forces, $g(\eta)$, force and torque input from the actuators, τ , and unknown disturbances. Gravitational and buoyancy forces are function of orientation of the vehicle since gravitational force affects the vehicle downwards, $+z$, and buoyancy force affects the vehicle upwards, $-z$, in earth fixed frame. However, the equation of motion, equation 4.22, is written in body fixed frame. Therefore, coordinate transform matrices will be used.

Gravitational force, f_G is related to the weight of the vehicle, $W = mg$, where m is mass of the vehicle and g is the gravitational acceleration.

$$f_G = {R_{321}}^{-1}(\eta)\begin{bmatrix} 0 \\ 0 \\ W \end{bmatrix} \tag{4.44}$$

Buoyancy force, f_B is related to the weight of the vehicle, $B = \rho g \nabla$, where ρ is density of the fluid and ∇ is volume of the vehicle.

$$f_B = -{R_{321}}^{-1}(\eta)\begin{bmatrix} 0 \\ 0 \\ B \end{bmatrix} \tag{4.45}$$

Gravitational and buoyancy forces are combined in $g(\eta)$, and can be written as below.

$$g(\eta) = \begin{bmatrix} f_G + f_B \\ r_G \times f_G + r_B \times f_B \end{bmatrix} \tag{4.46}$$

where $r_G = [x_G \quad y_G \quad z_G]^T$ is the center of gravity and $r_B = [x_B \quad y_B \quad z_B]^T$ is the center of buoyancy. Substituting the equations 4.44 and 4.45, into 4.46 gives,

$$(\eta) = \begin{bmatrix} (W-B)sin\theta \\ -(W-B)cos\theta sin\varphi \\ -(W-B)cos\theta cos\varphi \\ -(y_G W - y_B B)cos\theta cos\varphi + (z_G W - z_B B)cos\theta sin\varphi \\ (z_G W - z_B B)sin\theta + (x_G W - x_B B)cos\theta cos\varphi \\ -(x_G W - x_B B)cos\theta sin\varphi - (y_G W - y_B B)sin\theta \end{bmatrix} \tag{4.47}$$

The vehicle has four propellers which can produce forces and moments in four DOFs, surge, pitch, heave, and yaw. Force and torque input vector τ can be expressed as

$$\tau = LU \tag{4.48}$$

where U is a vector of inputs from propellers

$$U = \begin{bmatrix} U_1 \\ U_2 \\ U_3 \\ U_4 \end{bmatrix} \tag{4.49}$$

L is the propeller mapping matrix which is used to find the effect of propellers in body fixed frame. Figure 4.2 shows the positions of propeller inputs and helps to derive the mapping matrix.

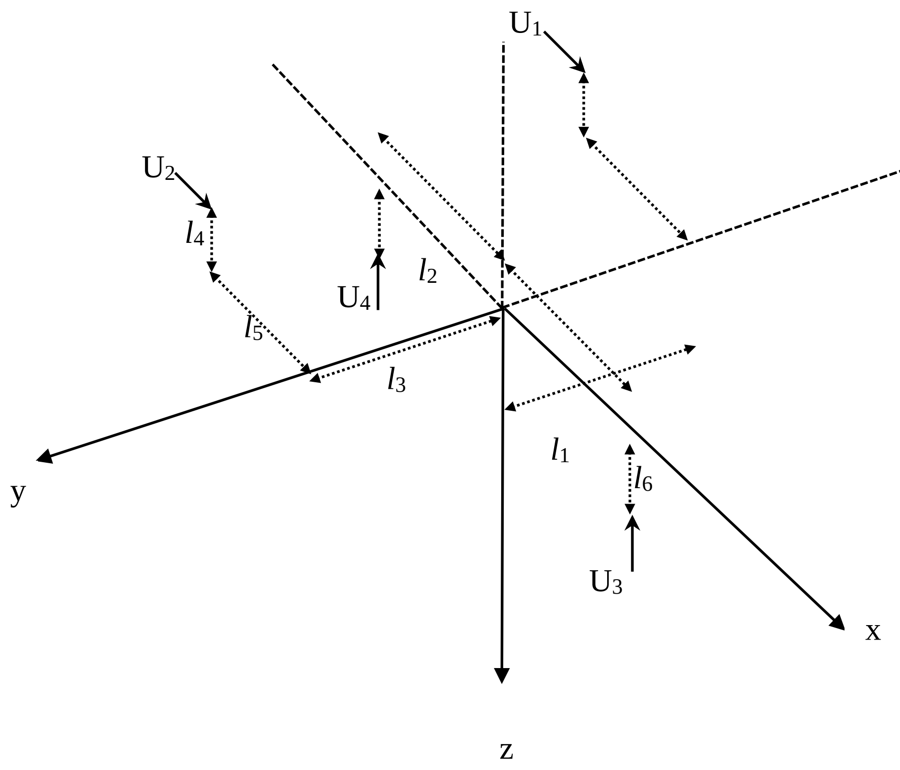

Figure 4.3. Diagram of propeller position for use of mapping matrix

The mapping matrix L is given by

$$L = \begin{bmatrix} 1 & 1 & 0 & 0 \\ 0 & 0 & 0 & 0 \\ 0 & 0 & 1 & 1 \\ 0 & 0 & 0 & 0 \\ -l_4 & -l_4 & l_1 & -l_2 \\ l_3 & -l_3 & 0 & 0 \end{bmatrix}, \; L \epsilon \mathbb{R}^{6\times 4} \tag{4.50}$$

The task of finding the required propeller input for determined forces and moments in body-fixed frame, is an inverse problem which can be carried out below equations.

$$U = L^{+}\tau \tag{4.51}$$

$$L^{+} = (L^{T}L)^{-1}L^{T} \tag{4.52}$$

It should be noted, there is no possible input to create sway and roll motion, since the second and fourth rows of the mapping matrix are all zero.

5. PARAMETER ESTIMATION AND DYNAMIC SIMULATION

In this chapter model parameters and dynamic simulations are presented. In section 5.1 assumptions and parameters introduced. Parameters are obtained analytically. In section 5.2 dynamic simulations carried out. First, behavior of the vehicle observed with different propeller input. Then, stabilization of the vehicle is simulated. Finally, reference positions defined to analyze the controllability of the model. The results of simulations are discussed.

5.1. Model Parameters

The numerical simulations of the vehicle will be carried out with the help of the kinematic and dynamic model, which is presented in the previous section, and reasonably accurate model parameters. The complexity of the kinematic and dynamic model is reduced with multiple assumptions.

5.1.1. Assumptions

As mentioned above following assumptions are made for the sake of simplicity which will result in healthier simulations.

- The vehicle operates in a relatively low speed, maximum of 1 m/s, which allows to neglect lift forces.
- The vehicle is symmetric in all three planes, which implies the shape of the vehicle assumed to be rectangular prism. This assumption can be made due to first assumption.
- The vehicle stays close to horizontal due to positions of actuators and centers of buoyancy and gravity are aligned with respect to surge direction, which results in that roll and pitch movements can be neglected.
- The origin of the body fixed frame is positioned at the center of gravity.
- The vehicle is assumed to operate in enclosed water thus environmental disturbances are neglected.
- The degrees of freedom are decoupled which means the degrees of freedom do not affect each other. This assumption is valid due to symmetry assumption and neglection of environmental disturbances. Decoupling results in Coriolis and centripetal matrices becomes negligible.

After assumptions dynamic model reduces into

$$M\dot{\nu} + D(\nu)\nu \ + g(\eta) = \ \tau \tag{5.1}$$

5.1.2. Parameters

Parameter estimation of underwater vehicles is performed in multiple methods in previous works. These methods include using computer softwares and experimental methods. In this work accurate expression for parameters are derived with the help of (Fossen, 1994) and (Tang, 1999)

<u>Mass and Inertia</u>

The mass and inertia matrix in the equation 5.1 consists of two parts, M_{RB}, constant inertia matrix of rigid body and M_A, added mass matrix. M_{RB} is given in equation 4.31 and the numerical values are defined with the use of SolidWorks.

$$m = 27{,}385\ kg \tag{5.2}$$

$$I_{xx} = 235073{,}453\ kgmm^2 \tag{5.3}$$

$$I_{yy} = 213350{,}814\ kgmm^2 \tag{5.4}$$

$$I_{zz} = 234702{,}781\ kgmm^2 \tag{5.5}$$

For the added mass matrix, given in equation 4.38, strip theory is applied with rectangular cross section. The principle of strip theory is defining two dimensional hydrodynamic coefficients for cross sectional areas and summarizing over the body via integrating. Added mass terms is found as given below.

$$X_{\dot{u}} = -\int_{-\frac{L}{2}}^{\frac{L}{2}} A_{11}^{(2D)}(y,z)dx \approx -0.1m \tag{5.6}$$

$$Y_{\dot{v}} = -\int_{-\frac{L}{2}}^{\frac{L}{2}} A_{22}^{(2D)}(y,z)dx \tag{5.7}$$

$$Z_{\dot{w}} = -\int_{-\frac{L}{2}}^{\frac{L}{2}} A_{33}^{(2D)}(y,z)dx \tag{5.8}$$

$$K_{\dot{p}} = -\int_{-\frac{B}{2}}^{\frac{B}{2}} y^2 A_{33}^{(2D)}(x,z)dy - \int_{-\frac{H}{2}}^{\frac{H}{2}} z^2 A_{22}^{(2D)}(x,y)dz \tag{5.9}$$

$$M_{\dot{q}} = -\int_{-\frac{L}{2}}^{\frac{L}{2}} x^2 A_{33}^{(2D)}(y,z)dx - \int_{-\frac{H}{2}}^{\frac{H}{2}} z^2 A_{11}^{(2D)}(x,y)dz \tag{5.10}$$

$$N_{\dot{r}} = -\int_{-\frac{B}{2}}^{\frac{B}{2}} y^2 A_{11}^{(2D)}(x,z)dy - \int_{-\frac{L}{2}}^{\frac{L}{2}} x^2 A_{22}^{(2D)}(y,z)dx \tag{5.11}$$

Where L, B, and H are the main dimensions of the vehicle. The cross-sectional areas of the vehicle are rectangle and constant in all dimensions. For rectangle cross sections, the graph in figure 4 can be used.

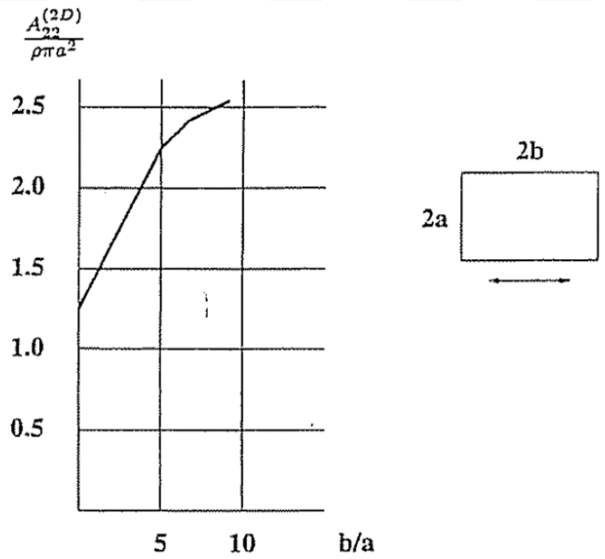

Figure 5.1. Two-dimensional added mass coefficient for rectangular cross section

The ratio b/a is between 0 and 5 for all dimensions therefore the following expression can be obtained.

$$A_{ii}^{(2D)} = \frac{4\frac{b}{a} + 25}{20} \rho\pi a^2 \tag{5.12}$$

Employing above formula for cross section areas in three dimensions, with the density of water 10^{-6} kg/mm^3

$$A_{11}^{(2D)} = 0.02165\ kg/mm \tag{5.13}$$

$$A_{22}^{(2D)} = 0.02259\ kg/mm \tag{5.14}$$

$$A_{33}^{(2D)} = 0.17811\ kg/mm \tag{5.15}$$

Substituting the values in equations 5.13-15, into equations 5.6-11 numerical values of added mass is found as below.

$$X_{\dot{u}} = -0.1m \tag{5.16}$$

$$Y_{\dot{v}} = -9.003\ kg \tag{5.17}$$

$$Z_{\dot{w}} = -21.373\ kg \tag{5.18}$$

$$K_{\dot{p}} = -942809.2557\ kgmm^2 \tag{5.19}$$

$$M_{\dot{q}} = -1026077.543\ kgmm^2 \tag{5.20}$$

$$N_{\dot{r}} = -243950.6985\ kgmm^2 \tag{5.21}$$

<u>Hydrodynamic Damping</u>

The damping matrix is investigated in two terms, linear and quadratic damping, as mentioned in previous chapter. The linear quadratic damping terms assumed to be zero due to alignment of center of gravity and center of buoyancy(Eidsvik & Schjølberg, 2016). In order to find quadratic damping terms equation 4.42 is employed.

$$X_{u|u|} = -\frac{1}{2}\rho C_D A \tag{5.22}$$

Where ρ is the density of water, C_D is the damping coefficient and A is the cross-sectional area which is perpendicular to the corresponding direction. Damping coefficient C_D is a function of Reynolds number which depends to speed of flow, in this case the speed of the velocity. Considering the operation circumcstances of vehicle the value of C_D is found in (Hoerner, 1951)(Hoerner, 1951) . The elements of damping matrix in surge, sway, and heave directions is given below.

$$X_{u|u|} = -0.2384\ kg/m \tag{5.23}$$

$$Y_{v|v|} = -0.2384\ kg/m \tag{5.24}$$

$$Z_{w|w|} = -0.2384\ kg/m \tag{5.25}$$

The problem of deriving the damping terms in roll, pitch, and yaw directions must be approached infinitesimally.

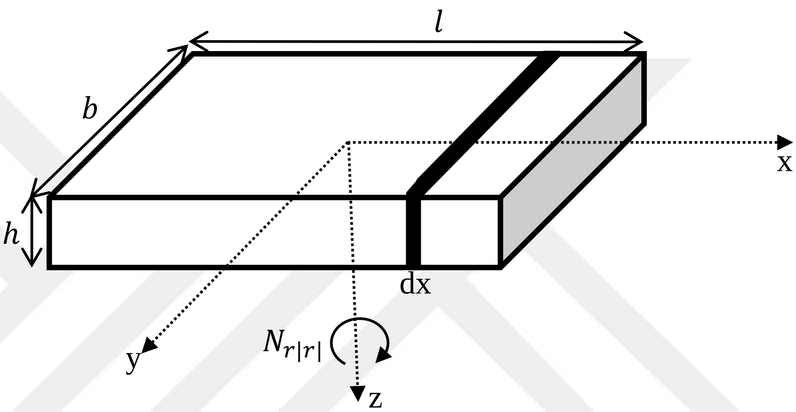

Figure 5.2. Infinitesimal analysis for the yaw damping

Considering the yaw damping as shown in Figure 4.4, the highlighted infinitesimal piece is rotating with angular speed r, during the yaw motion. The cross-sectional area subjected to toe motion is hdx. Equation 4.42 can be written as

$$f(r) = N_{r|r|}r|r| = -\frac{1}{2}\rho C_D U|U|x\int_{-l/2}^{l/2} hdx \tag{5.26}$$

Assuming small motions, the linear speed can be assumed to be perpendicular to cross-section. Hence, $U = rx$. The expression becomes

$$N_{r|r|} = -\frac{1}{2}\rho C_D x\int_{-l/2}^{l/2} hx^2 dx \tag{5.27a}$$

Similarly,

$$K_{p|p|} = -\frac{1}{24}\rho C_D l b^4 \tag{5.28}$$

$$M_{q|q|} = -\frac{1}{24}\rho C_D b h^4 \tag{5.29}$$

The elements of damping matrices given below

$$K_{p|p|} = -0.0043 \tag{5.30}$$

$$M_{q|q|} = -3.4331 \times 10^{-5} \tag{5.31}$$

$$N_{r|r|} = -0.0014 \tag{5.32}$$

External Forces and Moments

The bottom three terms in the vector of gravitional and buoyancy forces in equation 4.47 , become zero due to assumption of that the origin of the body fixed frame is located at center of gravity and buoyancy. The distances in mapping matrix in equation 4.50 is given by

$$l_1 = 145\ mm \tag{5.33}$$

$$l_2 = 135\ mm \tag{5.34}$$

$$l_3 = 132.85\ mm \tag{5.35}$$

$$l_4 = 12.5\ mm \tag{5.36}$$

5.2. Dynamic Simulation

Using the the kinematic and dynamic model derived in previous sections, dynamic simulation of the vehicle is carried out as if it is remotely operated, in other world open-loop control. Four main tasks are assigned which are namely free motion, upward-downward, backward-forward, and rotation motion. The mathematical model is defined in MATLAB software and simulation of four tasks are performed. For the solution ode4 function of MATLAB and state space representation is used. Defining the space vector as follows

$$\chi = [x\ \ u\ \ y\ \ v\ \ z\ \ w\ \ \varphi\ \ p\ \ \theta\ \ q\ \ \psi\ \ r]^T \tag{5.37}$$

Taking the derivative of space vector χ

$$\dot{\chi} = [u \quad \dot{u} \quad v \quad \dot{v} \quad w \quad \dot{w} \quad p \quad \dot{p} \quad q \quad \dot{q} \quad r \quad \dot{r}]^T \tag{5.38}$$

Now rearranging the equation 5.1

$$\dot{\nu} = \frac{\tau - D(\nu)\nu - g(\eta)}{M} \tag{5.39}$$

The MATLAB function ode4 solves this type of differential equations using Runge-Kutta method which is an iterative numerical method useful in solving differential equations where derivative of a function is also a function of itself. It divides the independent variable, time in this case, into intervals and iterates from initial point to end point. Through iteration derivative of the function is used which is the rate of change of the function by definition. In above equation time derivative of ν, $\dot{\nu}$, is a function of ν. The dynamic simulations are carried out considering the cases in which different combinations of propellers operate. The time passed is determined as 5 seconds with step-size of 10-4 seconds. The block diagram of the open-loop system given in Figure 5.3. Propeller inputs are given in Table 5.1

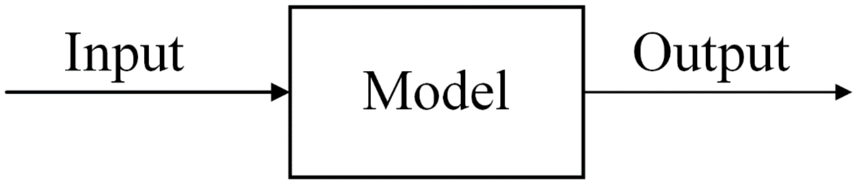

Figure 5.3. Block diagram of the open loop system

Table 5.1. Propeller inputs of the open loop system

Inputs (N) / Cases	U_1	U_2	U_3	U_4
Case 1	0	0	0	0
Case 2	5	5	0	0
Case 3	0	0	20	20
Case 4	5	5	25	25
Case 5	5	0	25	25

The first case is the case of no propeller working. The expectation is that the vehicle falls downwards, in other words, it moves in the heave direction. The results of the MATLAB simulation is given in Figures 5.4-6.

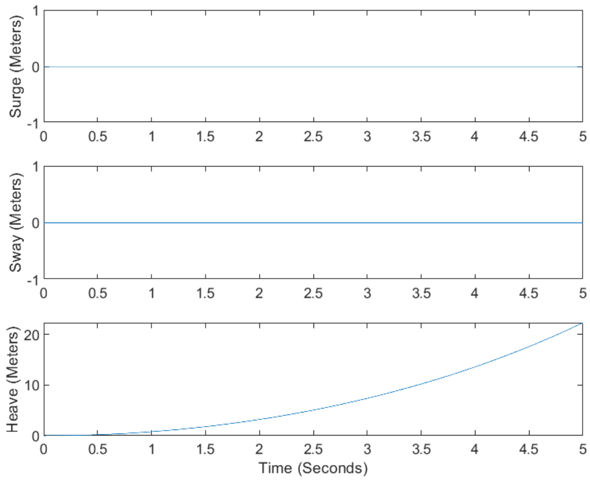

Figure 5.4. Surge, sway, and heave results of the simulation of first case

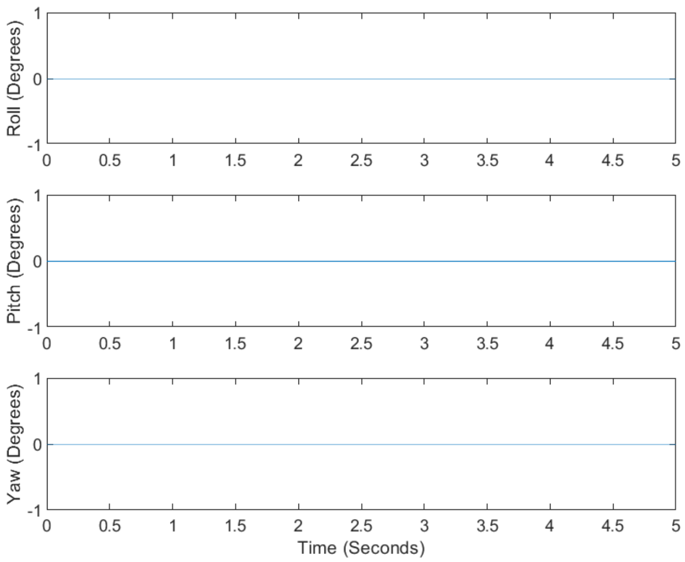

Figure 5.5. Roll, pitch, and yaw results of the simulation of the first case

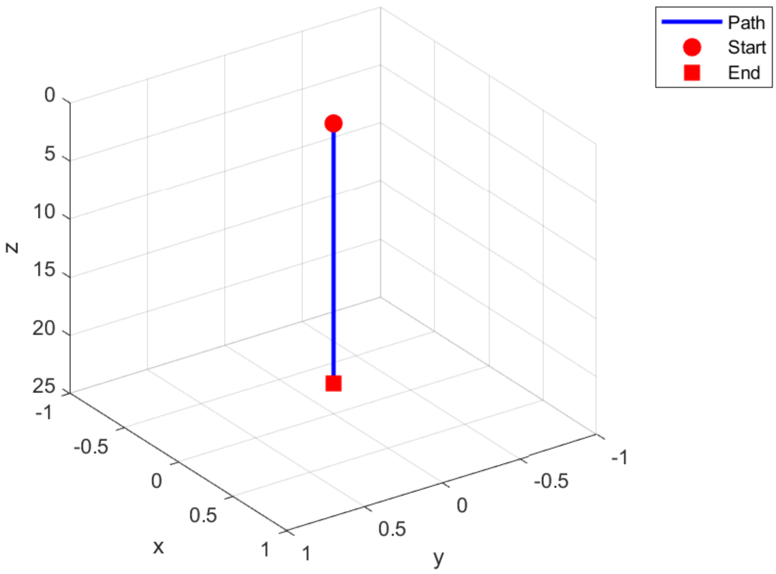

Figure 5.6. The motion of the first case in 3-D coordinate system

The second case is rear two propellers are working with the same input, 5N. These two propellers are anticipated to produce motion in surge direction. However, due to gravititational and buoyancy forces, the vehicle should also have motion in heave direction. The results are given in Figures 5.7-9.

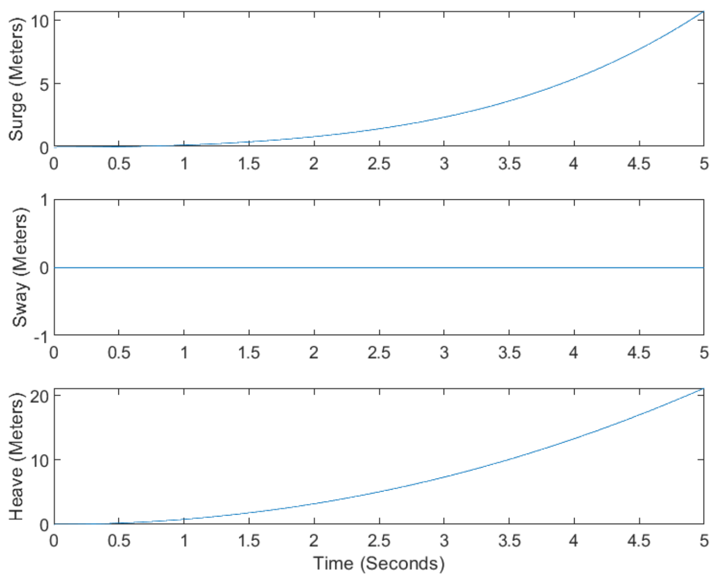

Figure 5.7. Surge, sway, and heave results of the simulation of the second case

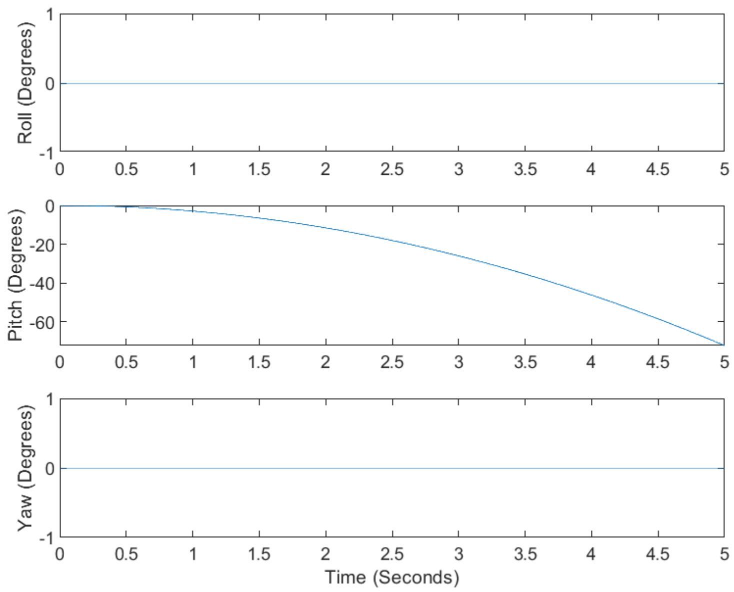

Figure 5.8 Roll, pitch, and yaw results of the simulation of the second case

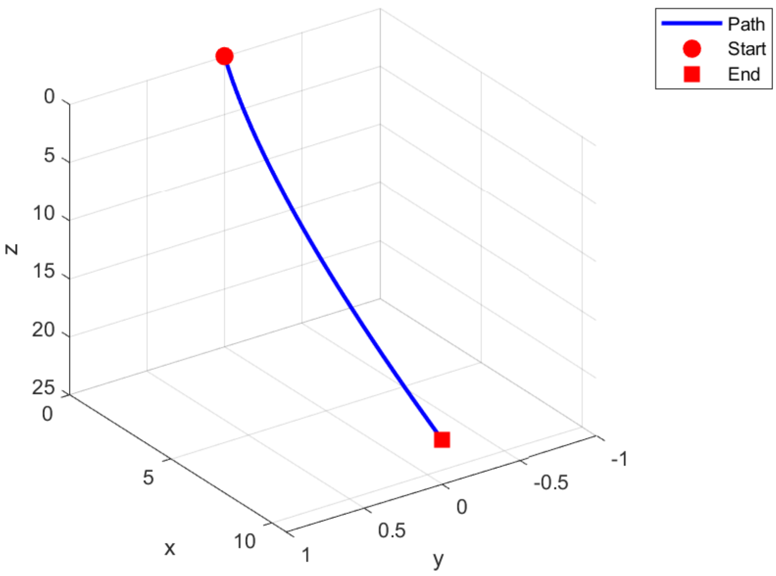

Figure 5.9. The motion of the second case in 3-D coordinate system

In the second case the acting forces are propeller forces in surge direction and gravitational and buoyancy forces in heave direction. Therefore, the vehicle moves forward and downward. Consequently, there is a rotation in pitch direction.

The third case is the trial of hanging the vehicle in the water. For such operation bottom propellers have to work. In the simulation, 20 N input is given to both bottom propellers. The results are shown in Figures 5.10-12.

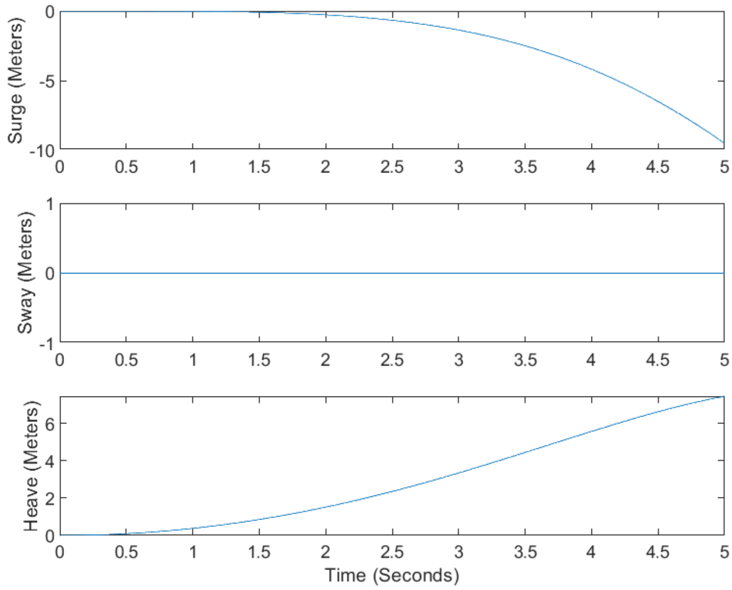

Figure 5.10. Surge, sway, and heave results of the simulation of the third case

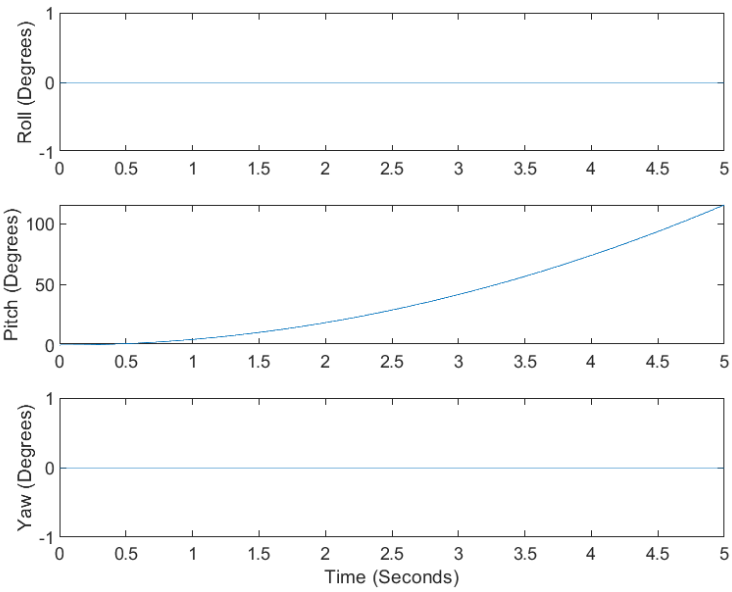

Figure 5.11. Roll, pitch, and yaw results of the simulation of the third case

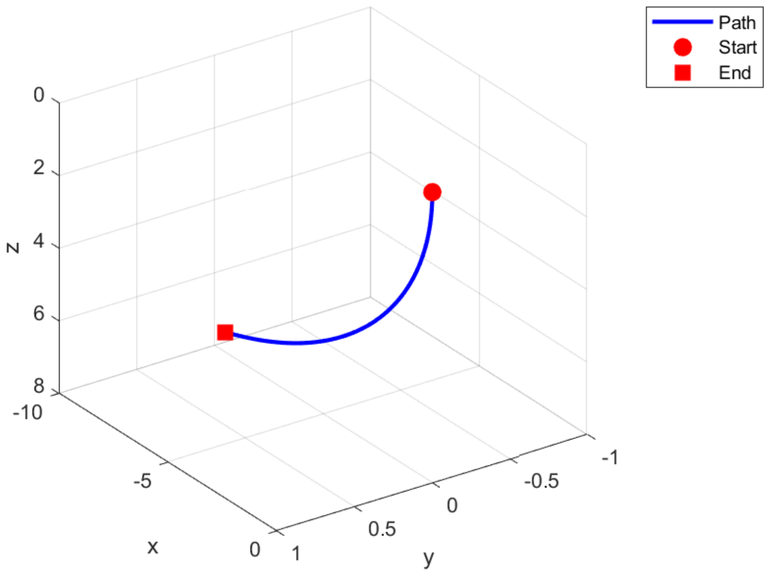

Figure 5.12. The motion of the third case in 3-D coordinate system

In the third case the inputs are not sufficient to keep the vehicle at constant heave value. This can be accomplished by control methods. Also there is an unexpected rotation in the pitch direction. Which results in a motion in negative surge direction since, after rotation, there is a surge component of the forces applied by bottom propellers. Pitch rotation is due to the difference between the distances of bottom proppellers to the center of gravity. Bottom-rear propeller is closer to the center of gravity than the bottom-front propeller. This feature also brings out the necessity of the use of control methods.

The fourth case is the trial of moving the vehicle forward without falling. In order to achieve the task, all four propellers must operate. From the information of the third case, 20 N input from bottom propellers is not enough to keep the vehicle level. Thus, an increased input of 25 N applied to the bottom propellers, whereas rear propeller inputs are 5 N. The results of simulation are given in Figures 5.13-15.

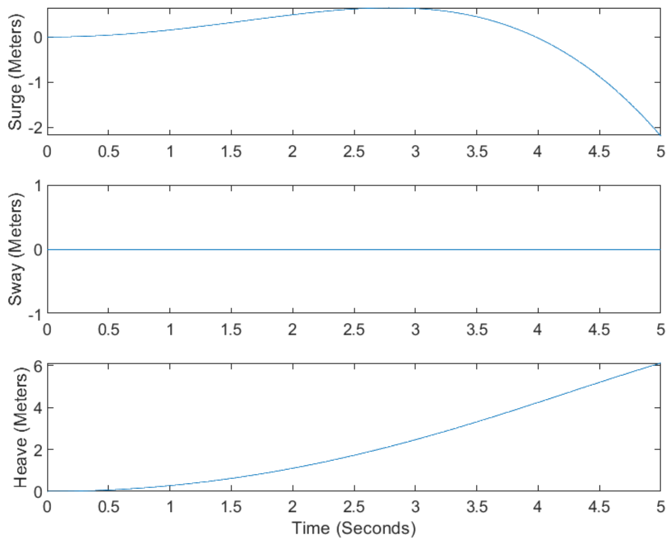

Figure 5.13. Surge, sway, and heave results of the simulation of the fourth case

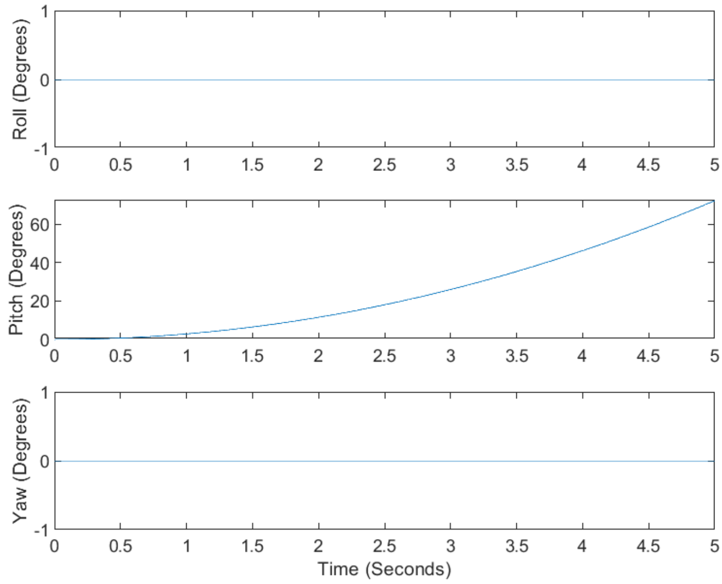

Figure 5.14. Roll, pitch, and yaw results of the simulation of the fourth case

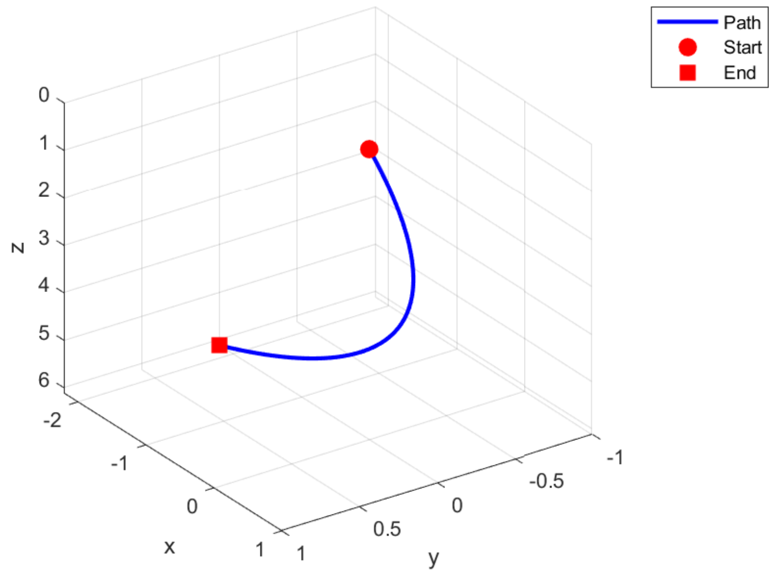

Figure 5.15. The motion of the fourth case in 3-D coordinate system

In the fourth case, results are far from success. For around 2.5 seconds of 5 second operation, the vehicle moves forward as intended. However, the second half of the operation is unsuccessful. Similar to previous cases, pitch rotation prevents desired results. The solution to this problem is giving varying inputs to the bottom propeller. Determining the varying inputs while the vehicle operates can be, again, managed by the use of control methods.

The fifth and the last case for dynamic simulation is rotating the vehicle to left or right, in other words, producing yaw rotation. The intuitional action is to give input to only one of the rear propellers. The vehicle will take a turn in the opposite direction of which rear propeller works. To carry out this task, 5 N input is given to the left propeller, expecting a turn to right which means a positive yaw rotation. The results of the simulation are given in Figures 4.16-18.

The results of the fifth case are not as expected. There is a rotation in yaw direction however the value is around 1000 degrees which means the vehicle rotates by itself two times. This issue can not be solved without eliminating the pitch rotation which is mentioned in previous cases. More healthy approach can be taken if the suspending the vehicle at a constant heave level is accomplished.

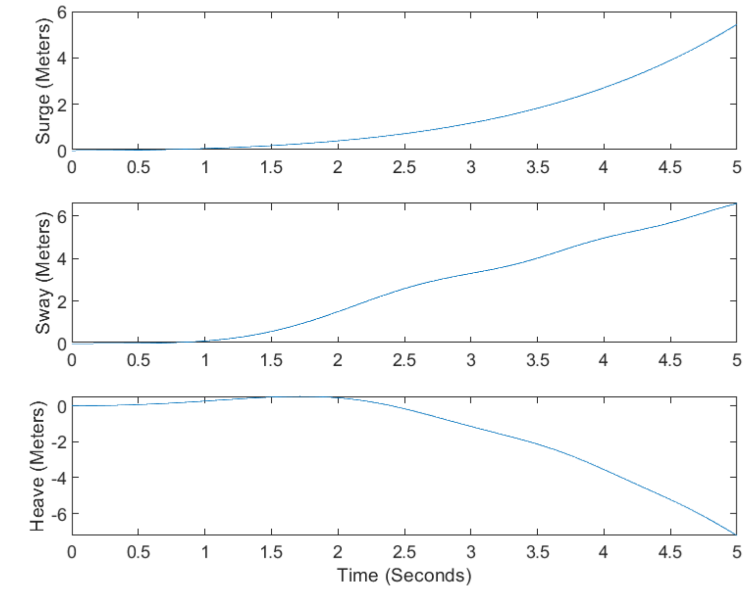

Figure 5.16. Surge, sway, and heave results of the simulation of the fifth case

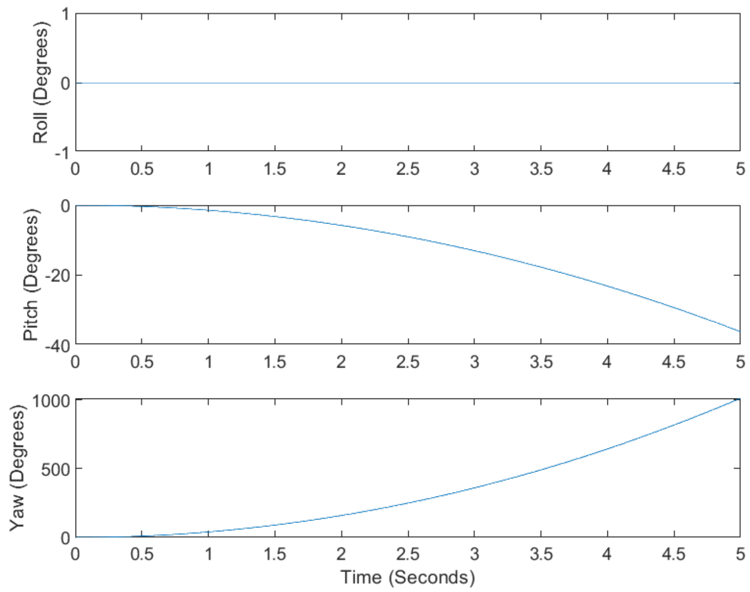

Figure 5.17. Roll, pitch, and yaw results of the simulation of the fourth case

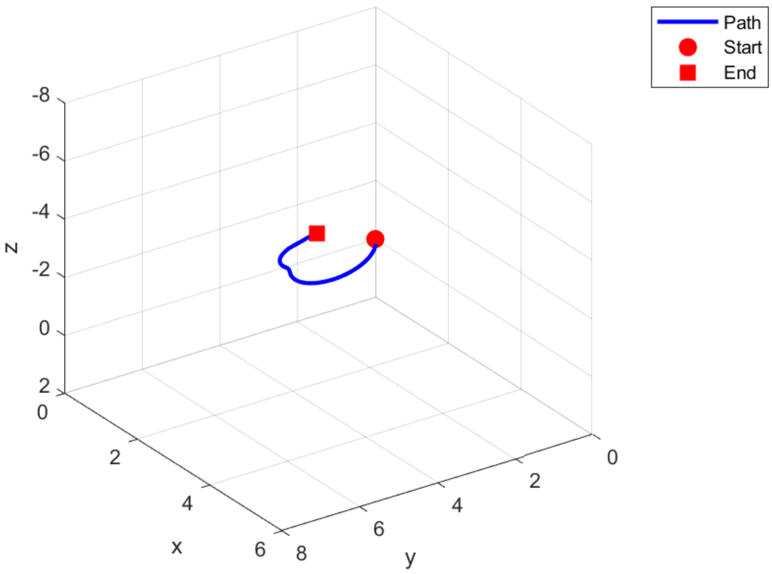

Figure 5.18. The motion of the fourth case in 3-D coordinate system

5.3. Control of the Unmanned Underwater Vehicles

Control of unmanned underwater vehicles is usually very complex due to their nonlinear dynamics. Considering the forces act on the vehicle such as hydrodynamic drag and lift forces, Coriolis and centripetal forces, gravity and buoyancy forces, and environmental disturbances, it becomes highly nonlinear equations of motions(Indiveri, 1998). Many degrees of this nonlinearity are left out due to the simplications and assumptions made in previous chapters. There are many control methods used for the control of unmanned underwater vehicles such as PID control, fuzzy logic control, adaptive control and sliding mode control. In this study PD control method is applied due to its easiness to implement linear systems.

5.3.1. Feedback Linearization

Considering the dynamic model derived in previous chapter, the coefficient matrices consist of diagonal terms. Therefore, each DOF can be investigated separately. One DOF equation of motion can be generalized as below.

$$m_x\ddot{x} = \tau_x - d_{\dot{x}|\dot{x}|}\dot{x}|\dot{x}| - g_x \quad (5.40)$$

Changing the coefficients

$$\ddot{x} = -a\dot{x}|\dot{x}| - b - c\tau_x \tag{5.41}$$

Where $a = \frac{d_{\dot{x}|\dot{x}|}}{m_x}$, $b = \frac{g_x}{m_x}$, $c = \frac{1}{m_x}$. Under steady-state conditions where $\ddot{x} = \dot{x} = 0$

$$0 = -b + c\tau_{x,SS}, \quad \tau_{x,SS} = \frac{b}{c} = g_x \tag{5.42}$$

The position is defined as output and system is rewritten as a single input single output (SISO) system.

$$\dot{x} = f(x) + g(x)u \tag{5.43a}$$
$$y = h(x) \tag{5.43b}$$

Where $u = \tau_x - \tau_{x,SS}$ is the control variable. Now define the state vector $X = [x_1\ x_2]^T = [x\ \dot{x}]^T$. Derivation of the state variables

$$\dot{x_1} = x_2 \tag{5.44a}$$
$$\dot{x_2} = -a\dot{x_2}|\dot{x_2}| - cu \tag{5.44b}$$

To eliminate nonlinearity, define the control variable u as

$$u = \frac{1}{c}(a\dot{x_2}|\dot{x_2}| + v) \tag{5.45}$$

State space system becomes

$$\dot{x_1} = x_2 \tag{5.46a}$$
$$\dot{x_2} = v \tag{5.46b}$$

With the exact knowledge of coefficient a, system is now rewritten linearly, where v is the linear state feedback control. Linearized system is rewritten as

$$X = A\dot{X} + Bv \tag{5.47}$$

Where $A = \begin{bmatrix} 0 & 1 \\ 0 & 0 \end{bmatrix}$ and $B = \begin{bmatrix} 0 \\ 1 \end{bmatrix}$. Setting $v = -KX$, where $K = [k_1 \quad k_2]$ and $k_{1,2} > 0$

$$X = (A - BK)\dot{X} \tag{5.48}$$

Such that $(A - BK)$ is Hurwitz in order to obtain an asymptotically stable system. $(A - BK)$ having the feature of Hurwitz, which means all eigenvalues smaller than zero, will make the state space vector X converge to a zero vector. In this case, position and velocity will be zero thus the vehicle will suspend in the water.

Overall, substituting the control laws v and u and steady state component $\tau_{x,SS}$, overall state feedback control law τ_x is derived to be

$$\tau_x = \frac{1}{c}(a\dot{x_2}|\dot{x_2}| + b - k_1x_1 - k_2x_2) \tag{5.49}$$

If this feedback control law is written in the 1-DOF equation of motion, we get

$$\ddot{x} + k_2\dot{x} + k_1x = 0 \tag{5.50}$$

Note that the solution of above differential equation is

$$x = c_1e^{\frac{\left(-k_2+\sqrt{{k_2}^2-4k_1}\right)t}{2}} + c_1e^{\frac{\left(-k_2-\sqrt{{k_2}^2-4k_1}\right)t}{2}} \tag{5.51}$$

Which always converge to zero as $t \to \infty$.

5.3.2. Reference Tracking

Feedback linearization, which is mentioned in the previous subsection, is useful when the task is keeping the vehicle at initial point, since it helps converge the position to zero. If the task is that the vehicle to follow a reference trajectory, r, state feedback control law τ_x must be defined by the use of error vector, e, which is given below with derivatives.

$$e = x - r \tag{5.52a}$$

$$\dot{e} = \dot{x} - \dot{r} \tag{5.52b}$$

$$\ddot{e} = \ddot{x} - \ddot{r} \tag{5.52c}$$

Defining the state vector as $E = [e_1\ e_2]^T = [\ e\ \dot{e}]^T$, if the feedback linearization is applied to E, position and velocity error will converge to zero. Thus, position and velocity will converge to corresponding reference values. The control law for reference tracking is given below.

$$\tau_x = d_{\dot{x}}\dot{x}|\dot{x}| + g_x + m_x\ddot{r} - m_x k_1 e - m_x k_2 \dot{e} \tag{5.53}$$

Note that, position, velocity and acceleration of the vehicle and reference signal is assumed to be known at any point of the operation. The coefficients k_1, k_2 is multiplied with error itself and derivative. Hence, the name PD (proportional-derivative) arises. An integral term $k_i \int e$ is added in order to eliminate the perturbations in the system such as waves a change in the mass of the vehicle. In this study integral term is not needed due to simplification of the system.

5.3.3. Dynamic Simulation with PD Control

In previous section, five cases in which the vehicle operates without any control method was presented. In this subsection, simulation with PD control of three cases which are counterpart of the first, the second and the fifth ones of the five cases in previous section. The block diagram of the simulation with PD control is given in Figure 5.19.

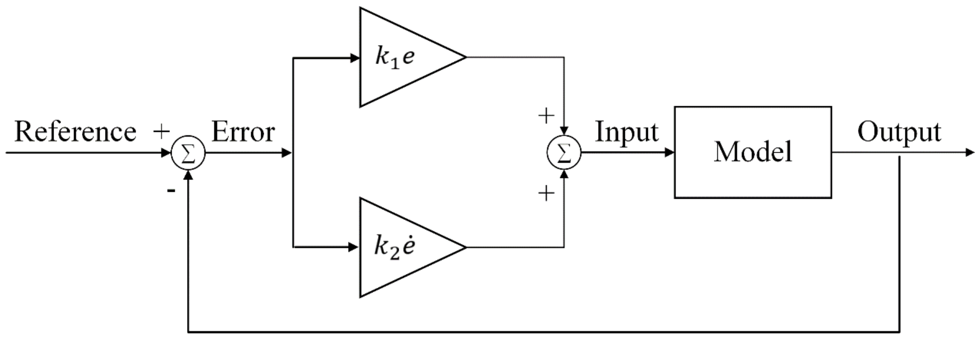

Figure 5.19. Block diagram of the simulation with PD control

The first case of the simulation of PD control is the task of leaving the vehicle hanging in the water, i.e., no position change in any direction. In previous section, when there was no propeller input, the vehicle, naturally, moved downwards due to the effect of gravity. With PD control, reference signal of the task is the same with initial point. The results of the simulation is given in figures 5.20-22.

As can be seen in the figures, the results are satisfying. There is no motion in any direction therefore the vehicle stays at the initial point. If the force applied to the vehicle through the simulation is investigation, it would be seen that there is a net force in the negative heave direction which balances the gravitational and buoyancy forces.

The second case is moving the vehicle in surge direction by setting a certain position of 5 meters. In the previous section, a similar case was giving inputs to rear propellers. Due to the gravitational forces the vehicle fell down while moving forward. With PD control, the ability of keeping the heave position of the vehicle same, will make the task successful. The simulation results are shown in figures 5.23-25.

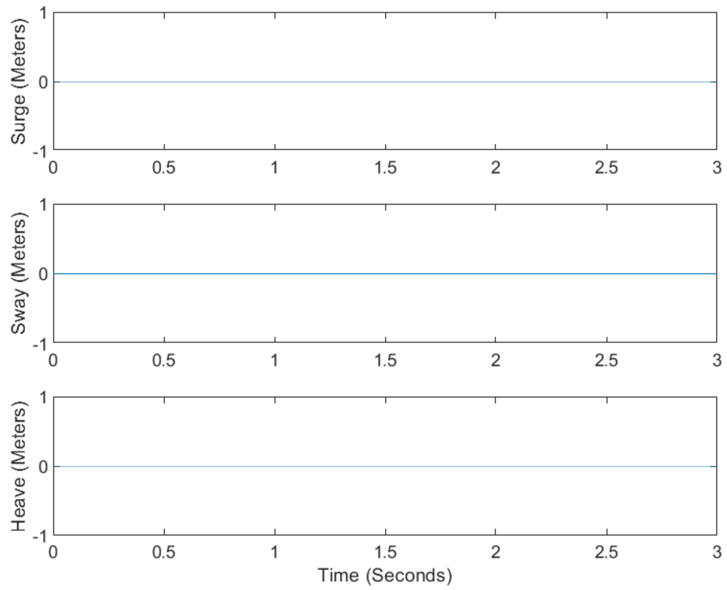

Figure 5.20. Surge, sway, and heave results of the simulation of the first case with PD control

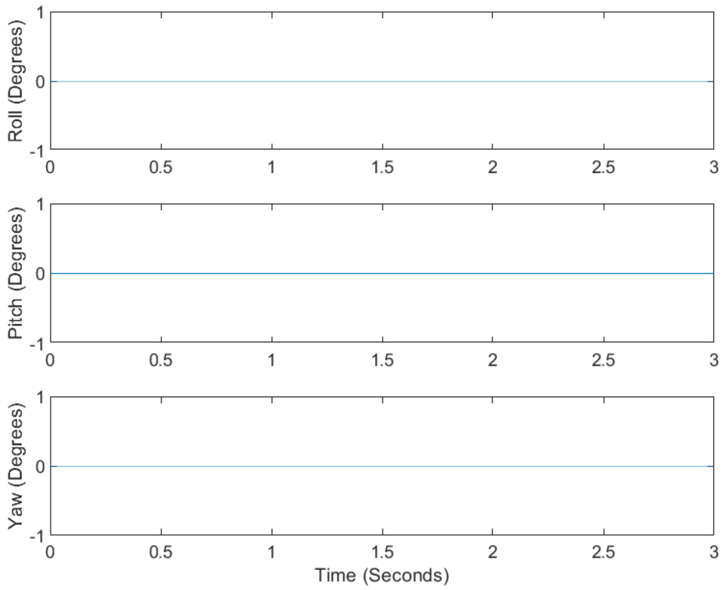

Figure 5.21. Roll, pitch, and yaw results of the simulation of the first case with PD control

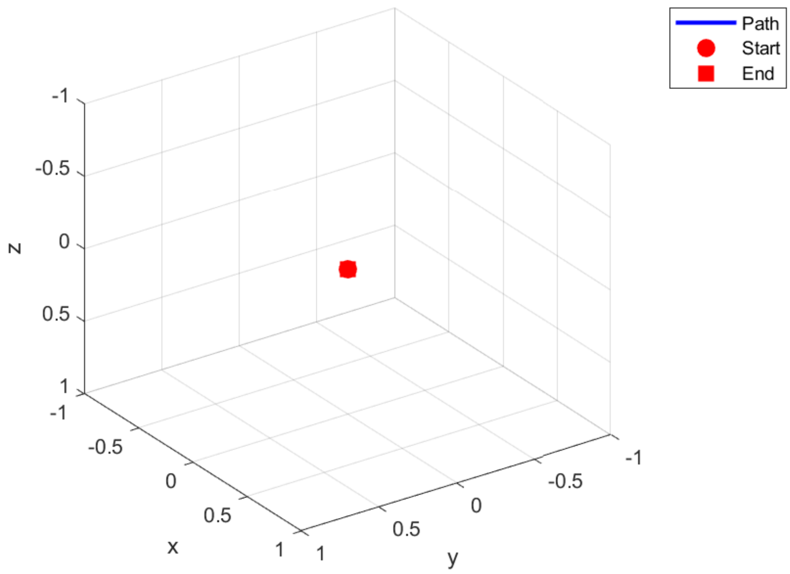

Figure 5.22. The motion of the first case with PD control in 3-D coordinate system

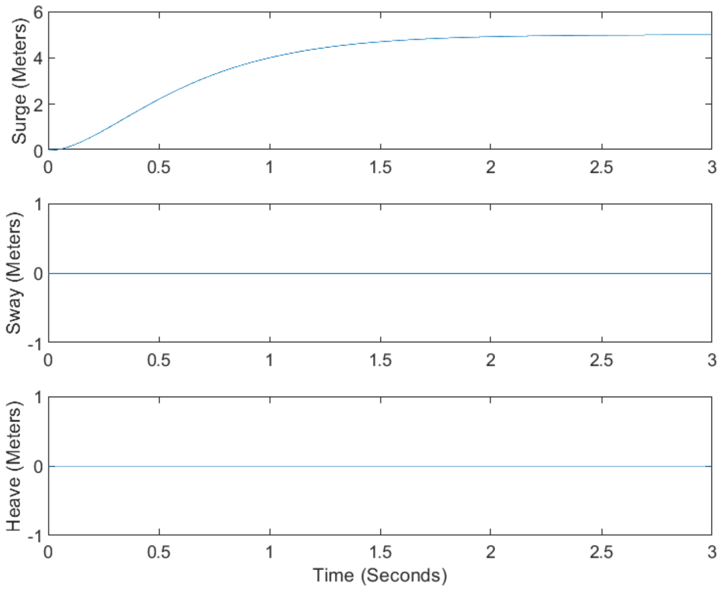

Figure 5.23. Surge, sway and heave results of the simulation of the second case with PD control

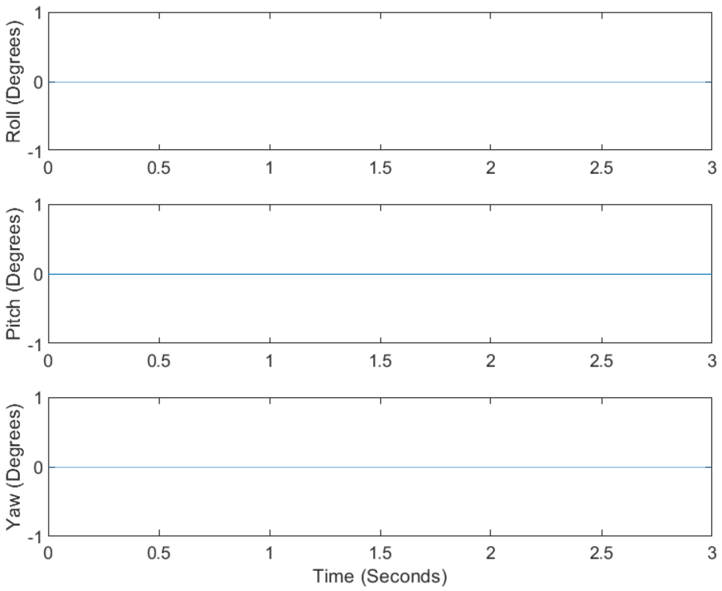

Figure 5.24. Roll, pitch, and yaw results of the simulation of the second case with PD control

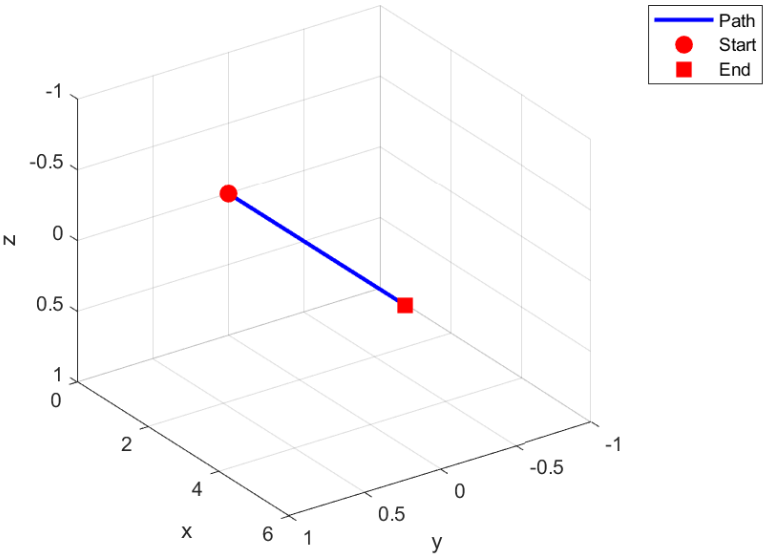

Figure 5.25. The motion of the second case with PD control in 3-D coordinate system

As expected, the vehicle stays at the same level while moving forward. It reaches the desired surge value of 5 in around 2.5 minutes. However, this time can be reduced by tuning the control coefficients k_1, k_2 in equation 5.53.

The third and last case with the PD control is rotating the vehicle in heave direction. For this simulation reference value of heave is given in 90^o and surge and sway positions -3 and 3 meters respectively. The results are given in figures 5.26-28.

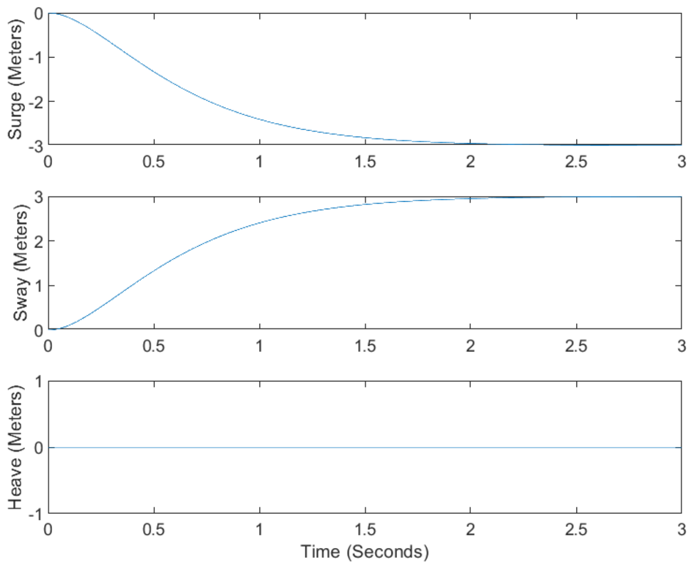

Figure 5.26. Surge, sway and heave results of the simulation of the third case with PD control

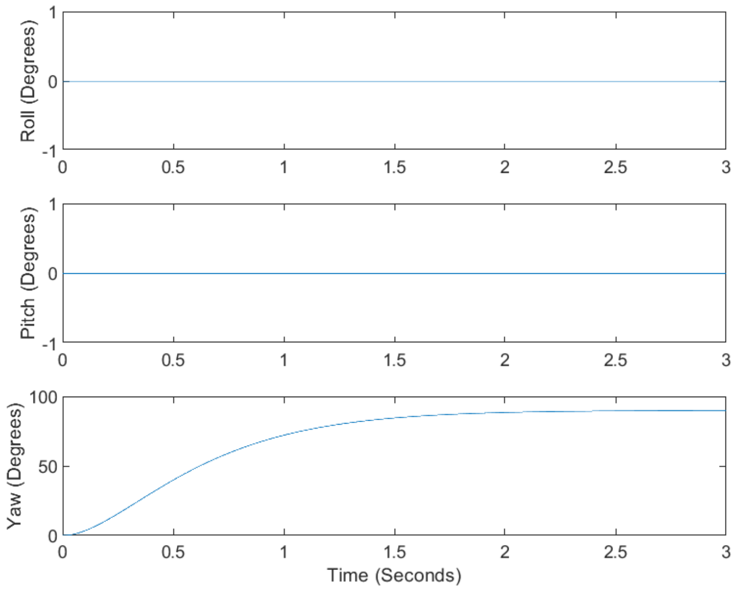

Figure 5.27. Roll, pitch, and yaw results of the simulation of the third case with PD control

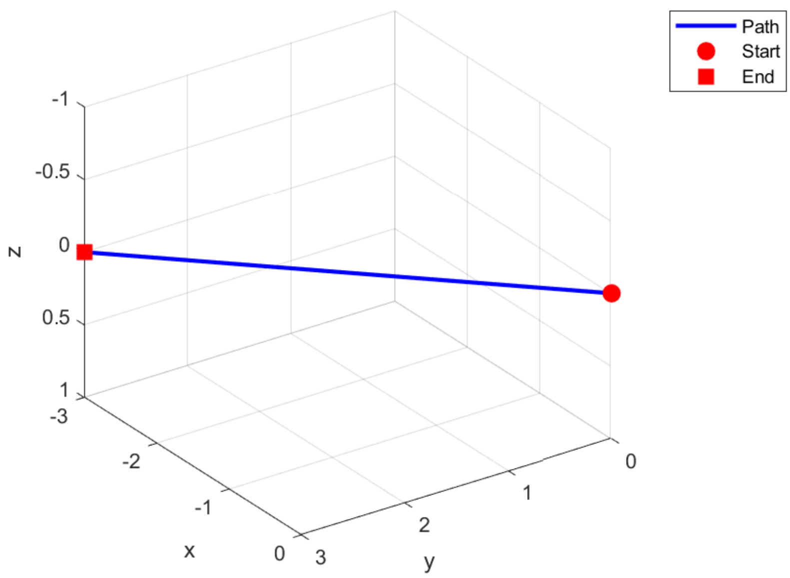

Figure 5.28. The motion of the third case with PD control in 3-D coordinate system

In the results of the third case simulation, vehicle can reach the defined values with success. However, a straight motion while rotating is not a realistic outcome. One of the reasons of this motion is simplification of the mathematical model of the vehicle and neglection of any disturbances. The other reason is the simulation with PD control is carried out by only calculating the needed net force applied by the propellers. The needed net forces and torques in all six degrees of freedom are given in Table 5.2. It is essential to check whether propellers can supply these net forces and torques. In order to do so, equation 4.51 must be used. Block diagram of simulation with propeller input is given in Figure 5.29.

Table 5.2. The needed net forces and torques with PD control

		Case 1	Case 2	Case 3
Surge	Reference (m)	0	5	-3
	Final position (m)	0	5	-3
	Needed net force (N)	0	1355	-813
Sway	Reference (m)	0	0	3
	Final position (m)	0	0	3
	Needed net force (N)	0	0	982
Heave	Reference (m)	0	0	0
	Final position (m)	0	0	0
	Needed net force (N)	-76.678	-76.678	-76.678
Roll	Reference (^{o})	0	0	0
	Final position (^{o})	0	0	0
	Needed net torque (Nm)	0	0	0
Pitch	Reference (^{o})	0	0	0
	Final position (^{o})	0	0	0
	Needed net torque (Nm)	0	0	0
Yaw	Reference (^{o})	0	0	90
	Final position (^{o})	0	0	90
	Needed net torque (Nm)	0	0	6.76

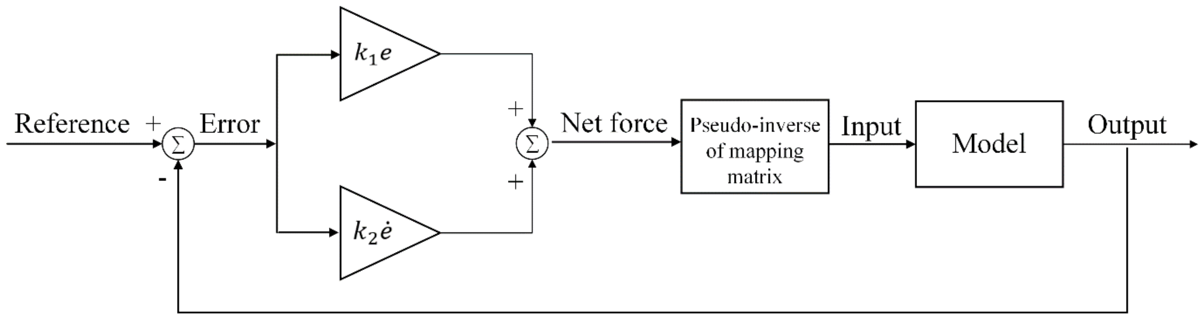

Figure 5.29. Block diagram of simulation with propeller input

Equation 4.51 helps to find input values for propellers to fulfill tasks mentioned above. When the equation included first and second case with PD control are carried out successfully. For the first case in which the vehicle simulation results show that vehicle can suspend in the initial point. When the input propeller values investigated, it is seen that bottom propellers work to overcome the gravitational and buoyancy forces however with different force values due to the difference of the distance to the center of gravity. Simulation results are shown in figures 5.30-32.

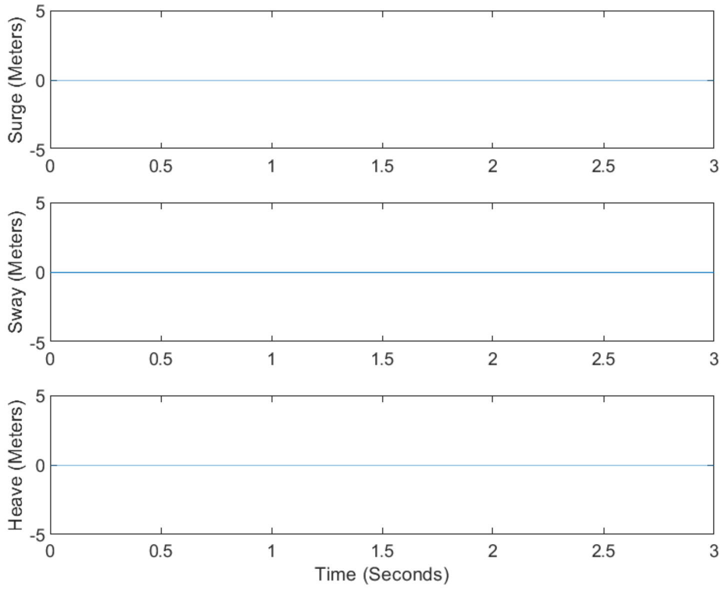

Figure 5.30. Surge, sway and heave results of the simulation of the first case with propeller input

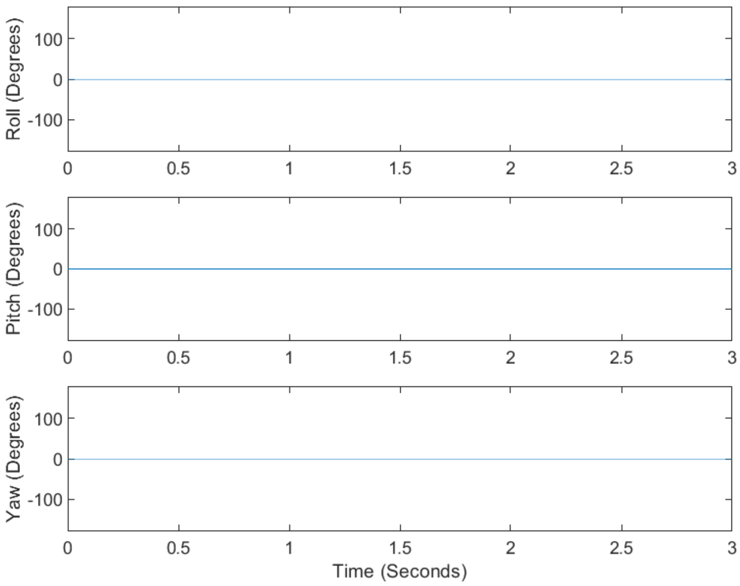

Figure 5.31. Roll, pitch and yaw results of the simulation of the first case with propeller input

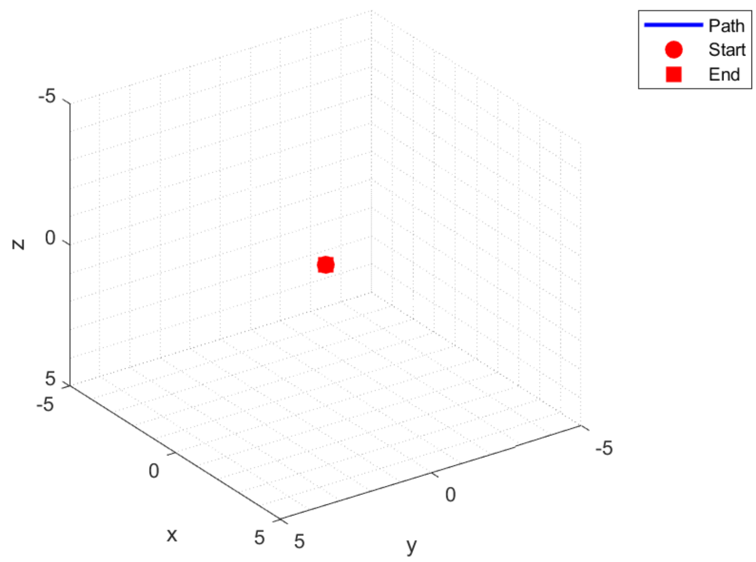

Figure 5.32. The motion of the third case with propeller inputs in 3-D coordinate system

The second case is the task of moving vehicle to a certain position of 3 meters in surge direction. Propeller inputs are all present for all four propellers, bottoms for suspension and rears for translation. The bottom propellers have a difference from above case since rear propellers also contribute to pitch rotation. In other words all propellers works in a way that vehicle stays in zero angular positions. The simulation results are given in figures 5.33-35

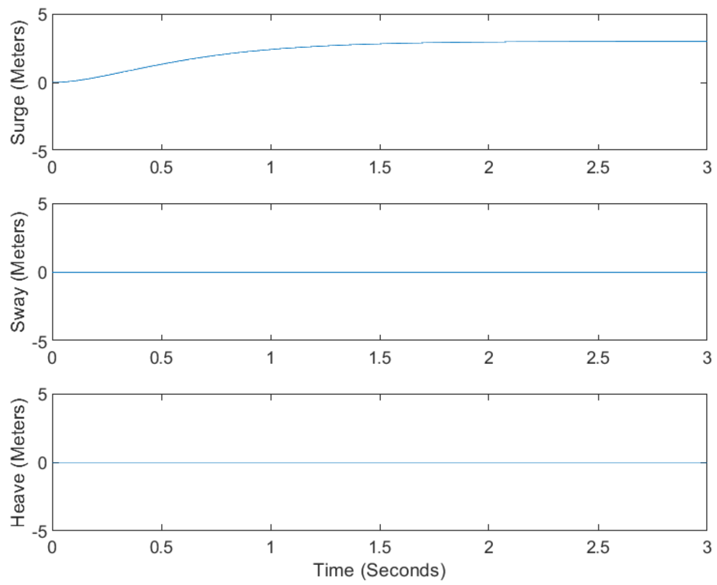

Figure 5.33. Surge, sway and heave results of the simulation of the second case with propeller input

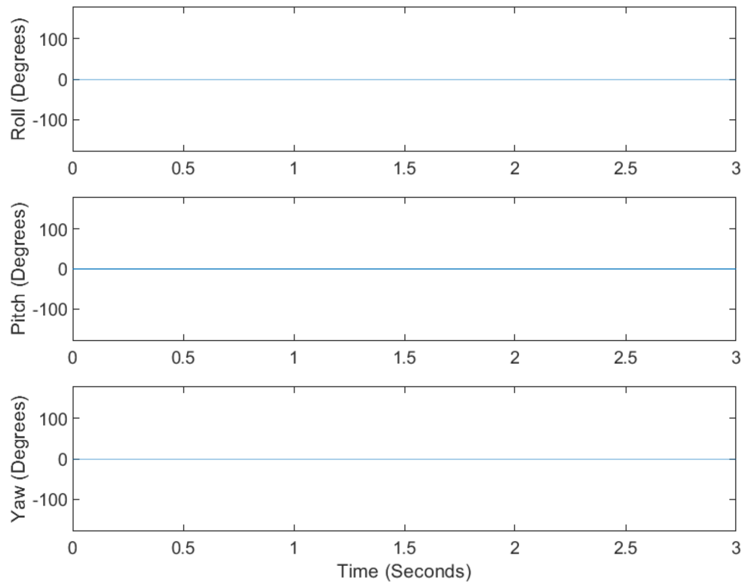

Figure 5.34. Roll, pitch and yaw results of the simulation of the second case with propeller input

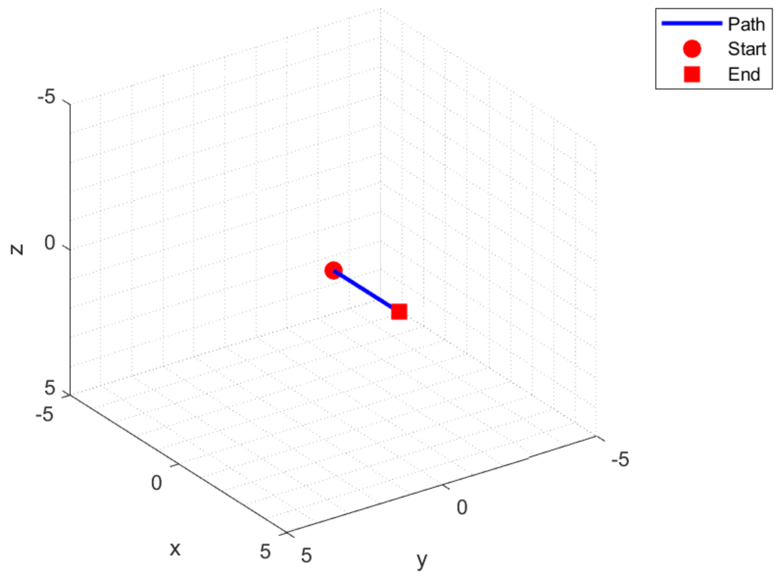

Figure 5.35. The motion of the second case with propeller inputs in 3-D coordinate system

The third and final case of the simulation with propeller inputs is rotating the vehicle 90^0 degrees and moving -3 and 3 meters in surge and sway directions respectively. This task is crucial since as mentioned in Chapter 4, there is no available input for the sway motion. The simulation results show that the vehicle is able to stay in x-y plane, However, although it manages to reach to the reference point it does not stop the rear vehicles as it supposed to do.

There is convergence in surge and yaw directions, but there is none in sway direction. This situation proves the vehicles inability to produce control inputs in sway direction. The results are shown in figures 5.36-38.

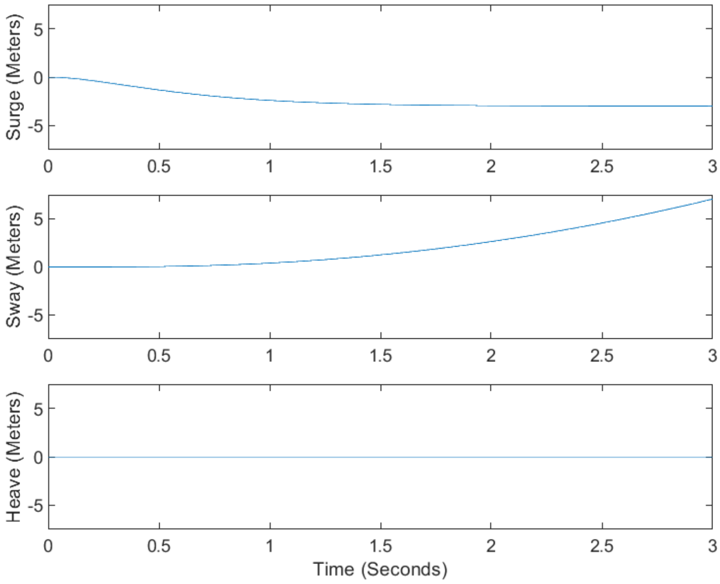

Figure 5.36. Surge, sway and heave results of the simulation of the third case with propeller input

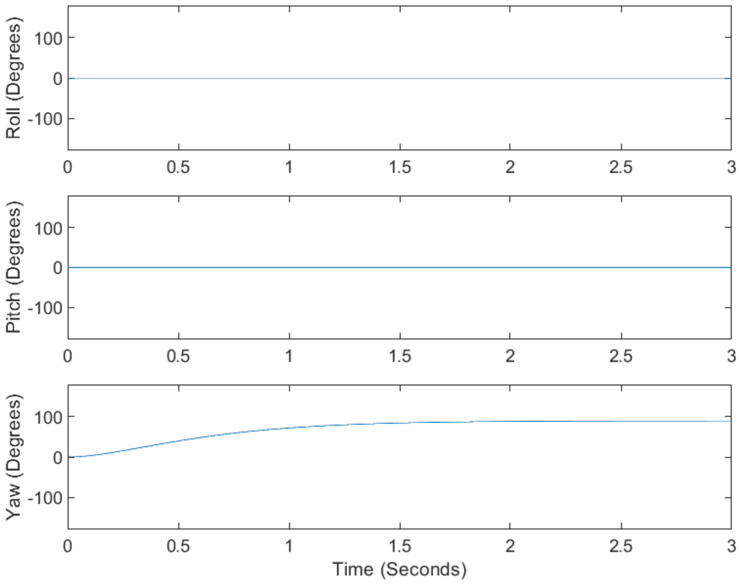

Figure 5.37. Roll, pitch and yaw results of the simulation of the third case with propeller input

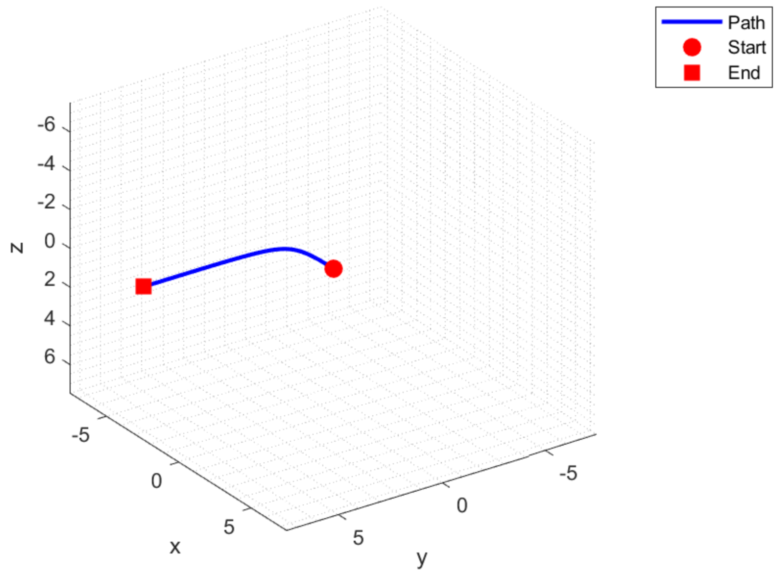

Figure 5.38. The motion of the third case with propeller inputs in 3-D coordinate system

The propeller inputs are given in Table 5.3. Note that the inability of motion in sway direction causes problem finding propeller inputs for case 3. The problem that occurred in the third case of simulation with propeller inputs can be solved path planning methods. The vehicle may lead to the reference point by trailing a arc-like path which is predetermined, without needing sway motion. Also, in the presence of disturbances, an adaptive controller with observer estimator should be applied. Issues such as path planning and adaptive controller are left out of scope in this thesis.

Table 5.3. Computed propeller inputs

Inputs (N) / Cases	U_1	U_2	U_3	U_4
Case 1	0	0	37.1	39.8
Case 2	677.78	677.78	97.57	-20.71
Case 3	-381.2	-432.1	[0.75 , -36.2]	[76.1 , 36.3]

6. CONCLUSIONS

In this thesis, design, modelling and dynamics simulation of unmanned underwater vehicle is presented. Previous works in the are discussed with examples. The structure and geometry of the vehicle which is designed by bachelor students of Adana Alparslan Türkeş Science and Technology University is given. Detailed information about kinematics of an unmanned underwater vehicle is explained. Mathematical concepts such as earth fixed and body fixed frames, Euler angles, and rotation matrices are introduced. SNAME notation for frames is explained. 6-DOF dynamic model of the vehicle is presented and mass, Coriolis, centripetal and damping terms which are 6x6 matrices are clarified. Hydrodynamic effects of the water is deeply investigated. A mapping matrix is defined to estimate the force and moment effects of the propellers. The mapping matrix showed which of the 6-DOFs are controllable by propeller inputs. It is understood that sway and roll motions are not available to produce by the propellers due to their positions. In order to estimate the parameters of dynamic model, the vehicle assumed to operate at a low speed, is symmetric around all three axes and has coincident centers of gravity and buoyancy. After assumptions, the parameters of dynamics models are analytically derived. Using the parameters, dynamic simulations are carried out. First, the motion of the vehicle without any control methods is simulated. The positions and velocities in 6-DOF are defined to be a state vector which is used in ode4 function of MATLAB. Five different combinations of propeller inputs are tested. The motion of the vehicle was as expected thus the kinematic and dynamic model is considered to be accurate. In order to stabilize the vehicle, feedback linearization method is chosen. Theoretical background of the method is explained and implemented in MATLAB simulation. Three different constant reference positions are defined, and the behavior of the vehicle is observed. Results came out promising, mostly in keeping the vertical level of the vehicle constant. This section of simulation is run by deriving the net force needed to fulfill given tasks. In order to reach corresponding propeller inputs, pseudo-inverse of the derived net force is implemented. It is seen that the vehicle is successful at overcoming gravity and buoyancy and at moving forward. However, inability of motion in sway and pitch DOFs is shown.

In future, an asymmetric design of vehicle will be studied and manufactured. Analytical estimation of parameters will be supported by different techniques and computer software such as ANSYS and ADAMS. Considering the disturbances underwater, more complex control methods will be covered such as path planning, adaptive control etc. And finally, it is planned to implement designed controller to a microprocessor such as Raspbery Pi, and realization of the controller simulation will be carried out.

REFERENCES

Ahmad, F. F., Ghenai, C., Hamid, A. K., & Bettayeb, M. (2020). Application of sliding mode control for maximum power point tracking of solar photovoltaic systems: A comprehensive review. *Annual Reviews in Control*, *49*(xxxx), 173–196. https://doi.org/10.1016/j.arcontrol.2020.04.011

Allotta, B., Costanzi, R., Ridolfi, A., Salvetti, O., Reggiannini, M., Kruusmaa, M., Salumae, T., Lane, D. M., Frost, G., Tsiogkas, N., Cocco, M., Gualdesi, L., Lacava, G., Roig, D., Gundogdu, H. T., Dede, M. I. C., Baines, S., Tusa, S., Latti, P., & Scaradozzi, D. (2018). The ARROWS Project: Robotic technologies for underwater archaeology. *IOP Conference Series: Materials Science and Engineering*, *364*(1). https://doi.org/10.1088/1757-899X/364/1/012088

Alvarez, A., Caffaz, A., Caiti, A., Casalino, G., Clerici, E., Giorgi, F., Gualdesi, L., Turetta, A., & Viviani, R. (2005). Folaga: A very low cost autonomous underwater vehicle for coastal oceanography. In *IFAC Proceedings Volumes (IFAC-PapersOnline)* (Vol. 38, Issue 1). IFAC. https://doi.org/10.3182/20050703-6-cz-1902.01947

Baruch, A., Mazal, Y., Braginsky, B., & Guterman, H. (2020). Attitude Estimation of AUVs Based on a Network of Pressure Sensors. *IEEE Sensors Journal*, *20*(14), 7988–7996. https://doi.org/10.1109/JSEN.2020.2982607

Bejarbaneh, E. Y., Masoumnezhad, M., Armaghani, D. J., & Pham, B. T. (2020). Design of robust control based on linear matrix inequality and a novel hybrid PSO search technique for autonomous underwater vehicle. *Applied Ocean Research*, *101*(May), 102231. https://doi.org/10.1016/j.apor.2020.102231

Carreras, M., Hernandez, J. D., Vidal, E., Palomeras, N., Ribas, D., & Ridao, P. (2018). Sparus II AUV - A Hovering Vehicle for Seabed Inspection. *IEEE Journal of Oceanic Engineering*, *43*(2), 344–355. https://doi.org/10.1109/JOE.2018.2792278

Craven, P. J., Sutton, R., & Burns, R. S. (1998). Control strategies for unmanned underwater vehicles. *Journal of Navigation*, *51*(1), 79–105. https://doi.org/10.1017/S0373463397007601

Cristi, R., Papoulias, F. A., & Healey, A. J. (1990). Adaptive Sliding Mode Control of

Autonomous Underwater Vehicles in the Dive Plane. *IEEE Journal of Oceanic Engineering*, *15*(3), 152–160. https://doi.org/10.1109/48.107143

Desa, E., Madhan, R., Maurya, P., Navelkar, G., Mascarenhas, A., Prabhudesai, S., Afzulpurkar, S., & Bandodkar, S. (2007). The small Maya AUV - Initial field results. *International Ocean Systems*, *11*(1), 21351.

Diebel, J. (2006). Representing attitude: Euler angles, unit quaternions, and rotation vectors. *Matrix*, *58*, 1–35. ftp://sbai2009.ene.unb.br/Projects/GPS-IMU/George/arquivos/Bibliografia/79.pdf

Eidsvik, O. A., & Schjølberg, I. (2016). Determination of hydrodynamic parameters for remotely operated vehicles. *Proceedings of the International Conference on Offshore Mechanics and Arctic Engineering - OMAE*, *7*, 1–10. https://doi.org/10.1115/OMAE2016-54642

El-Hawary, F. (2000). The ocean engineering handbook. In *The Ocean Engineering Handbook*. CRC Press. https://doi.org/10.1201/9781420036732

Eldred, R., Lussier, J., & Pollman, A. (2021). Design and testing of a spherical autonomous underwater vehicle for shipwreck interior exploration. *Journal of Marine Science and Engineering*, *9*(3). https://doi.org/10.3390/jmse9030320

Fittery, A., Mazumdar, A., Lozano, M., & Asada, H. H. (2012). Omni-Egg: A smooth, spheroidal, appendage free underwater robot capable of 5 DOF motions. *OCEANS 2012 MTS/IEEE: Harnessing the Power of the Ocean*. https://doi.org/10.1109/OCEANS.2012.6404986

Fossen, T. I. (1994). *Guidance and Control of Ocean Vehicles*. Wiley.

Gan, W., Zhu, D., Hu, Z., Shi, X., Yang, L., & Chen, Y. (2020). Model predictive adaptive constraint tracking control for underwater vehicles. *IEEE Transactions on Industrial Electronics*, *67*(9), 7829–7840. https://doi.org/10.1109/TIE.2019.2941132

Harris, Z. J., & Whitcomb, L. L. (2021). Cooperative acoustic navigation of underwater vehicles without a DVL utilizing a dynamic process model: Theory and field evaluation. *Journal of Field Robotics*, *38*(5), 700–726. https://doi.org/10.1002/rob.22008

Hoerner, S. F. (1951). *Aerodynamic Drag: Practical Data on Aerodynamic Drag Evaluated and Presented* (p. 259). https://books.google.nl/books?id=bF78Qg8XVb8C

Hong, E. Y., Soon, H. G., & Chitre, M. (2010). Depth control of an autonomous underwater vehicle, STARFISH. *OCEANS'10 IEEE Sydney, OCEANSSYD 2010*. https://doi.org/10.1109/OCEANSSYD.2010.5603566

Hu, K., Chen, X., Weng, L., Tian, L., & Hu, Y. (2020). A Survey of Deep Neural Network Sliding Mode Control in Robot Application. *Proceedings - 2020 Chinese Automation Congress, CAC 2020*, 6659–6662. https://doi.org/10.1109/CAC51589.2020.9327212

Indiveri, G. (1998). *Modelling and Identification of Underwater Robotic Systems*.

Jacobi, M. (2015). Autonomous inspection of underwater structures. *Robotics and Autonomous Systems*, *67*, 80–86. https://doi.org/10.1016/j.robot.2014.10.006

Kato, N. (1994). " Aqua Explorer 1000 " for Inspection of Underwater Cables. *Behaviour*, 135–140.

Katzschmann, R. K., DelPreto, J., MacCurdy, R., & Rus, D. (2018). Exploration of underwater life with an acoustically controlled soft robotic fish. *Science Robotics*, *3*(16), 1–13. https://doi.org/10.1126/SCIROBOTICS.AAR3449

Kou, L., Xiang, J., Li, Y., & Bian, J. (2018). Stability and nonlinear controllability analysis of a quadrotor-like autonomous underwater vehicle considering variety of cases. *International Journal of Advanced Robotic Systems*, *15*(6), 1–10. https://doi.org/10.1177/1729881418819401

Li, Y., Guo, S., & Wang, Y. (2017). Design and characteristics evaluation of a novel spherical underwater robot. *Robotics and Autonomous Systems*, *94*, 61–74. https://doi.org/10.1016/j.robot.2017.03.014

Liu, H., Lyu, Y., Lewis, F. L., & Wan, Y. (2019). Robust time-varying formation control for multiple underwater vehicles subject to nonlinearities and uncertainties. *International Journal of Robust and Nonlinear Control*, *29*(9), 2712–2724. https://doi.org/10.1002/rnc.4517

Marani, G., Choi, S. K., & Yuh, J. (2009). Underwater autonomous manipulation for intervention missions AUVs. *Ocean Engineering*, *36*(1), 15–23. https://doi.org/10.1016/j.oceaneng.2008.08.007

McMahon, J., & Plaku, E. (2016). Mission and motion planning for autonomous underwater vehicles operating in spatially and temporally complex environments. *IEEE Journal of Oceanic Engineering*, *41*(4), 893–912. https://doi.org/10.1109/JOE.2015.2503498

Panish, R., & Taylor, M. (2011). Achieving high navigation accuracy using inertial navigation systems in autonomous underwater vehicles. *OCEANS 2011 IEEE - Spain*. https://doi.org/10.1109/Oceans-Spain.2011.6003517

Pio, R. L. (1966). Euler Angle Transformations. *IEEE Transactions on Automatic Control*, *11*(4), 707–715. https://doi.org/10.1109/tac.1966.1098430

Prats, M., Ribas, D., Palomeras, N., García, J. C., Nannen, V., Wirth, S., Fernández, J. J., Beltrán, J. P., Campos, R., Ridao, P., Sanz, P. J., Oliver, G., Carreras, M., Gracias, N., Marín, R., & Ortiz, A. (2012). Reconfigurable AUV for intervention missions: A case study on underwater object recovery. *Intelligent Service Robotics*, *5*(1), 19–31. https://doi.org/10.1007/s11370-011-0101-z

Roper, D. T., Sharma, S., Sutton, R., & Culverhouse, P. (2011). A review of developments towards biologically inspired propulsion systems for autonomous underwater vehicles. *Proceedings of the Institution of Mechanical Engineers Part M: Journal of Engineering for the Maritime Environment*, *225*(2), 77–96. https://doi.org/10.1177/1475090210397438

Sahoo, A., Dwivedy, S. K., & Robi, P. S. (2019). Advancements in the field of autonomous underwater vehicle. *Ocean Engineering*, *181*(April), 145–160. https://doi.org/10.1016/j.oceaneng.2019.04.011

Sato, Y., Maki, T., Matsuda, T., & Sakamaki, T. (2015). Detailed 3D seafloor imaging of Kagoshima Bay by AUV Tri-TON2. *2015 IEEE Underwater Technology, UT 2015*. https://doi.org/10.1109/UT.2015.7108314

Shi, Y., Shen, C., Fang, H., & Li, H. (2017). Advanced control in marine mechatronic systems: A survey. *IEEE/ASME Transactions on Mechatronics*, *22*(3), 1121–1131. https://doi.org/10.1109/TMECH.2017.2660528

Shome, S. N., Nandy, S., Pal, D., Das, S. K., Vadali, S. R. K., Basu, J., & Ghosh, S. (2012). Development of Modular Shallow Water AUV: Issues & Trial Results. *Journal of The Institution of Engineers (India): Series C*, *93*(3), 217–228. https://doi.org/10.1007/s40032-012-0026-0

Siciliano, B., & Khatib, O. (2008). *Springer Handbook of Robotics*. Springer.

SNAME. (1950). *Nomenclature for Treating the Motion of a Submerged Body Through a Fluid*.

Tang, S. C. (1999). *Modeling and simulation of the autonomous underwater vehicle, Autolycus*. 129.

Tijjani, A. S., Chemori, A., & Creuze, V. (2022). A survey on tracking control of unmanned underwater vehicles: Experiments-based approach. *Annual Reviews in Control*, *54*(June), 125–147. https://doi.org/10.1016/j.arcontrol.2022.07.001

Vervoort, J. H. A. M. (2009). *Modeling and Control of an Unmanned Underwater Vehicle*. University of Canterbury.

Widditsch, H. (n.d.). *SPURV-the First Decade*.

Yang, G. H., Choi, W., Lee, S. H., Kim, K. S., Lee, H. J., Choi, H. S., & Ryuh, Y. S. (2011). Control and design of a 3 DOF fish robot "Ichtus." *2011 IEEE International Conference on Robotics and Biomimetics, ROBIO 2011*, 2108–2113. https://doi.org/10.1109/ROBIO.2011.6181603

Yang, R., Clement, B., Mansour, A., Li, M., & Wu, N. (2015). Modeling of a Complex-Shaped Underwater Vehicle for Robust Control Scheme. *Journal of Intelligent and Robotic Systems: Theory and Applications*, *80*(3–4), 491–506. https://doi.org/10.1007/s10846-015-0186-2

Zemouche, A., Zhang, F., Mazenc, F., & Rajamani, R. (2019). High-Gain Nonlinear Observer With Lower Tuning Parameter. *IEEE Transactions on Automatic Control*, *64*(8), 3194–3209. https://doi.org/10.1109/TAC.2018.2882417

Zhang, J., Han, G., Sha, J., Qian, Y., & Liu, J. (2022). AUV-Assisted Subsea Exploration Method in 6G Enabled Deep Ocean Based on a Cooperative Pac-Men Mechanism. *IEEE*

Transactions on Intelligent Transportation Systems, *23*(2), 1649–1660. https://doi.org/10.1109/TITS.2021.3102995

Zhao, C., & Guo, L. (2021). Control of Nonlinear Uncertain Systems by Extended PID. *IEEE Transactions on Automatic Control*, *66*(8), 3840–3847. https://doi.org/10.1109/TAC.2020.3030876

Zhu, D., & Sun, B. (2013). The bio-inspired model based hybrid sliding-mode tracking control for unmanned underwater vehicles. *Engineering Applications of Artificial Intelligence*, *26*(10), 2260–2269. https://doi.org/10.1016/j.engappai.2013.08.017